Supplement to January/ February 2023
Volume 52, Number 1

AppliedRadiology®
The Journal of Practical Medical Imaging and Management

Leaders on the Horizon Residents' Program 2022

Magnetic Resonance Imaging

Supported by Bracco Diagnostics, Inc.

Applied Radiology®

The Journal of Practical Medical Imaging and Management

Anderson Publishing, Ltd
180 Glenside Avenue,
Scotch Plains, NJ 07076
Tel: 908-301-1995
Fax: 908-301-1997
info@appliedradiology.com

PRESIDENT & CEO
Oliver Anderson

GROUP PUBLISHER
Kieran N Anderson

EDITOR-IN-CHIEF
Erin Simon Schwartz, MD, FACR

EXECUTIVE EDITOR
Joseph F Jalkiewicz

PRODUCTION
Barbara A Shopiro

FOREWORD

We at *Applied Radiology*, along with Bracco Diagnostics, Inc., are pleased to announce the winning authors in the 2022 "Leaders on the Horizon" Residents' Program, which challenged radiology residents to submit clinical research papers on topics related to MRI. The following five residents from around the country are this year's winners:

1. Jordan Chamberlin, MD, Medical University of South Carolina
2. Alexander Satei, MD, Trinity Health Oakland–Wayne State University
3. Melina Hosseiny, MD, University of California San Diego
4. Moozhan Nikpanah, MD, University of Alabama at Birmingham
5. Akarshan Monga, MD, Detroit Medical Center

In addition to earning the publication of their papers in this special supplement to *Applied Radiology*, the winners received scholarship awards to further their career in their respective fields of interest. Further, the residents were invited to attend the 2022 Radiological Society of North America Scientific Meeting and Exhibition, where they were honored at a special reception on November 27, 2022.

Supported by Bracco Diagnostics, Inc., the "Leaders on the Horizon" Residents' Program champions the next generation of radiology leaders. The program offers residents the opportunity to be recognized for their outstanding clinical research while expanding their knowledge of the imaging industry. This program is a key component of *Applied Radiology's* and Bracco Diagnostics' ongoing commitment to advancing medical imaging knowledge, leadership, and education.

Underpinning this program was a distinguished review board comprising ten expert radiologists and educators from various sub-specialties of radiology who judged all of the submissions and ultimately selected the top five papers. The reviewers were: Lorna Browne, MD; Christopher Comstock, MD; Mark C. DeLano, MD, FACR; Paul Finn, MD; Alessandro Furlan, MD; Christine Glastonbury, MBBS; Ryan Lee, MD, MBA; Mahmud Mossa-Basha, MD; Neil Rofsky, MD; and Frank Shellock, PhD, FACR, FACC, FISMRM.

For information about the "Leaders on the Horizon" Residents' Program, visit: appliedradiology.com/leaders.

LEADERS ON THE HORIZON 2022

Jordan Chamberlin, MD
Medical University
of South Carolina

Normative Left Ventricular Segmental T2 Mapping Values and Relationship With Cardiac Function In Patients With Cardiac Sarcoidosis **4**

Alexander M Satei, MBBS
Wayne State University
School of Medicine

Review of Clinically Significant Cancer in Lesions Labeled PI-RADS 3 on MRI Using PI-RADS Version 2.1 **13**

Melina Hosseiny, MD
University of California
San Diego

Multitasking Neural Networks for Multiplanar MRI Prostate Localization and Segmentation **20**

Moozhan Nikpanah, MD
University of Alabama
at Birmingham

Low Versus Ultra-High Field MRI: How to Select Your MRI Fleet **28**

Akarshan Monga, DO
Detroit Medical Center

Improving Radiology Resident Proficiency in MRI Safety **42**

Normative Left Ventricular Segmental T2 Mapping Values and Relationship With Cardiac Function in Patients With Cardiac Sarcoidosis

Jordan Chamberlin, MD[1†]; Ismail M. Kabakus, MD, PhD[1]; Madison R. Kocher, MD[1]; Gilberto Aquino, MD[1]; Jeffrey Waltz, MD[1]; Natalie Stringer, MD[1]; D. Jameson Dennis, MD[2]; Andrew Wortham, BS[1]; Akos Varga-Szemes, MD, PhD[1]; William Reiter, MD[1]; W. Ennis James, MD[3,4]; Brian A. Houston, MD[2,4]; Dhiraj Baruah, MD[1]; Andrew D. Hardie, MD[1]; Jeremy R. Burt, MD[1]

Abstract

Objective and Hypothesis: Cardiac sarcoidosis (CS) is a difficult-to-diagnose complication of systemic sarcoidosis. T2 mapping is a radiation and contrast-free examination, but the normative values and correlation with important function metrics are not well described. The authors hypothesize segmental T2 values will provide additional information about disease course.

Materials Methods: In this retrospective case-control study 55 sequential patients with sarcoidosis who underwent 1.5T gadolinium enhanced cardiac magnetic resonance imaging for suspected CS had American Heart Association left ventricular segmental T2 values and MRI-derived cardiac function measurements performed. The ground truth was defined as patients who were defined as "At least probable" by the 2019 WASOG criteria for cardiac sarcoidosis.

Results: 32 patients met WASOG "at least probable" criteria. All left ventricular segments had higher T2 mapping values in patients with cardiac sarcoidosis. Segment medians were 48.9 – 51.4 msec in patients with CS vs 46.3 – 47.9 msec in those without. The median ejection fraction (EF) for CS patients was 62% vs 68% for those without CS. Cardiac sarcoidosis patients in this study had significantly elevated end-systolic volume (ESV) (56mL vs 39 mL, P = 0.002). All T2 segment measurements were negatively correlated with ejection fraction (R = -0.64 to -0.78) in patients with reduced EF, but only middle and apical segments were positively correlated with increased end systolic function (R = 0.31, 0.31).

Conclusions: Median segmental T2 values for CS ranged from 48.9 – 51.4 msec. Patients with CS present with a 6% lower EF than their noncardiac controls. Elevated apical and mid T2 values were positively correlated with worsening systolic function and all segments were strongly negatively correlated with decreased EF. T2 mapping positively differentiates cases of cardiac sarcoidosis and correlates with important cardiac functional measurements.

Keywords: Cardiac Sarcoidosis, Cardiac MRI, Heart Failure, Non-ischemic Cardiomyopathy

Affiliations: [1]Division of Cardiothoracic Imaging, Department of Radiology, Medical University of South Carolina, Charleston, SC; [2]Division of Pulmonary and Critical Care Medicine, Medical University of South Carolina, Charleston, SC; [3]Division of Cardiology, Medical University of South Carolina, Charleston, SC; [4]Susan Pearlstine Sarcoidosis Center of Excellence, Medical University of South Carolina, Charleston, SC
Corresponding author[†]: Jordan H. Chamberlin MD, Clinical Science Building, 96 Jonathan Lucas Street , Suite 210, MSC 323, Charleston, SC 29425, (chamberj@musc.edu)
Conflict of interest and support statement: The authors declare no competing interests and received no funding or external support for this work.
Prior publication: No prior publication of this data has occurred.
Data sharing statement: Deidentified patient data and imaging values are available from the corresponding author upon reasonable request.

Introduction

Cardiac sarcoidosis (CS) is present in up to 25% of patients with systemic sarcoidosis and represents a diagnostic challenge owing to the patchy distribution and paroxysmal flaring of disease.[1] Current diagnostic methods revolve around the use of fluorodeoxyglucose positron emission computed tomography (FDG-PET/CT) for detection of hypermetabolic foci in the myocardium, late gadolinium enhancement (LGE) on cardiac magnetic resonance (CMR) imaging for identification of fibrosis, T2 CMR imaging for detection of myocardial edema, or some combination thereof.[2-4] Notably, radiologic diagnosis is the standard of care as endomyocardial biopsy has a reported 20-30% sensitivity owing to the patchy nature of disease.[1,5]

Confounding the diagnostic approach are the drawbacks of each agent; use of gadolinium-based contrast is contraindicated in patients with severe chronic kidney disease due to risk of nephrogenic systemic fibrosis, and FDG-PET delivers a large radiation dose and is patient-dependent for adequate glycemic suppression of the myocardial metabolic signal.[6,7] FDG-PET is most avidly used for diagnosis of active myocardial inflammation due to the larger body of literature supporting normative values and distribution of myocardial metabolism, while MRI largely identifies LGE as chronic cardiac sarcoidosis due to the pathology of interest being myocardial fibrosis, which is not present in the acute setting.[4,8] Notably, substantial overlap occurs in acute-on-chronic cases of CS, where active myocardial inflammation is superimposed on a background of fibrosis and the variable chronicity of findings is not well described.[9,10]

Recently, T1 and T2 mapping of the left ventricular myocardium has gained traction for its theoretical use as an adjunct for diagnosis of CS due to the lack of contrast needed, lack of radiation, and ability to describe active and chronic sequelae of myocardial inflammation.[11] Multiple studies have shown utility in T2 mapping for active disease, describing normative whole-heart T2 values, which are significantly elevated in patients with CS.[11-14] Further studies correlate elevated T2 mapping values with important cardiac outcomes and demonstrate resolution of T2 signal with treatment initation.[3,15] Ultimately, CS does not have a uniform cardiac predilection, and instead has a predilection for the basal and inferior myocardial segments.[16] Therefore, it is reasonable to consider that regional and segmental variations in cardiac sarcoid, and hypothetically T2 mapping values, may have important implications for the diagnosis and prognostication of disease.

There is a lack of literature on the segmental variation and relevance to important cardiac measurements, limiting further characterization and radiologic-pathologic correlation of disease. Notably, T2 mapping can address this deficiency because of the standard short-axis, three-slice view of the left ventricle, which can be reconstructed according to American Heart Association (AHA) left ventricular segments.[17] Therefore, the purpose of this study is to identify normative values of the myocardium in patients with sarcoidosis who have undergone CMR for the investigation of cardiac involvement of disease and to determine the extent of relationship with important MRI-derived cardiac function metrics. The authors hypothesize that segmental T2 mapping values will correlate with important cardiac function metrics because T2 mapping measures extent of acute pathology in cardiac sarcoidosis.

Methods

Ethics Statement

In accordance with the Health Insurance Portability and Accountability Act of 1996, a study protocol was submitted to the institutional review board at the covering institution and was deemed to be IRB-review exempt due to its retrospective nature and the need for informed consent was waived. All data was stored on encrypted network databases and no patient identifiers were shared across platforms.

Study Design and Patient Cohort

For this retrospective case-control study all patients with sarcoidosis who underwent a cardiac magnetic resonance imaging study with T2 mapping series from 2017 to 2020 were queried at a single institution. Inclusion criteria included a clinical or pathologic diagnosis of systemic sarcoidosis and age > 18 years. Exclusion criteria included patients with amyloidosis, myocarditis, hemochromatosis, or severe pulmonary hypertension. Technical exclusion criteria included severe artifact (pacemaker, motion, etc.) or outside institution referrals without access to necessary demographic and medical records. The ground truth for CS was defined as patients meeting "at least probable" World Association for Sarcoidosis and Other Granulomatous Disorders (WASOG) revised criteria independent of T2 mapping.[18] Fifty-five patients were ultimately included who met the criteria; seven patients with incomplete records and four patients with severe pulmonary hypertension were excluded.

WASOG Criteria for the diagnosis of cardiac sarcoidosis

1. "Highly Probable" — Defined as patients with a positive endomyocardial biopsy (EMB) with no alternative cause. EMB was not performed in any of these subjects and is not routinely performed at the authoring institution owing to noted subpar diagnostic performance.
2. "At Least Probable" — Defined as one of the following:
   - i. Treatment responsive cardiomyopathy or atrioventricular nodal block
   - ii. Reduced LVEF in the absence of other clinical risk factors
   - iii. Spontaneous or inducible sustained ventricular tachycardia with no other risk factors
   - iv. Mobitz type II or third-degree heart block
   - v. Patchy uptake on dedicated cardiac 18-fluorodeoxyglucose positron emission tomography
   - vi. Delayed enhancement on cardiac magnetic resonance imaging
   - vii. Positive gallium uptake
   - viii. Perfusion defect

Table 1. Demographics and summary statistics as stratified by probable diagnosis of cardiac sarcoidosis by WASOG criteria.

N = 55	CARDIAC SARCOIDOSIS (N = 32)		NO CARDIAC SARCOIDOSIS (N = 23)	
	Median	**IQR**	**Median**	**IQR**
Age	56	18.8	53	14.5
	N	%	N	%
Sex				
Female	14	43.8	13	56.5
Male	18	56.2	10	43.5
Race				
Black	19	59.4	12	52.2
White	13	40.6	11	47.8
EF < 50%	8	25	0	0
Positive FDG-PET	15	46.9	0	0
LGE	29	90.6	1	4.3
Perfusion defect	3	9.4	0	0
Positive EMB	0	0	0	0
Ventricular arrythmia	3	9.4	0	0
2nd or 3rd degree AVB	5	15.6	0	23

IQR = Interquartile range, EF = ejection fraction, FDG-PET = 18-fluorodeoxyglucose positron emission tomography, LGE = Late gadolinium enhancement, EMB = endomyocardial biopsy, AVB = atrioventricular (node) block

Figure 1. Whole-heart T2 values stratified by diagnosis of cardiac sarcoidosis (A). Ejection fraction values stratified by cardiac sarcoidosis(B).

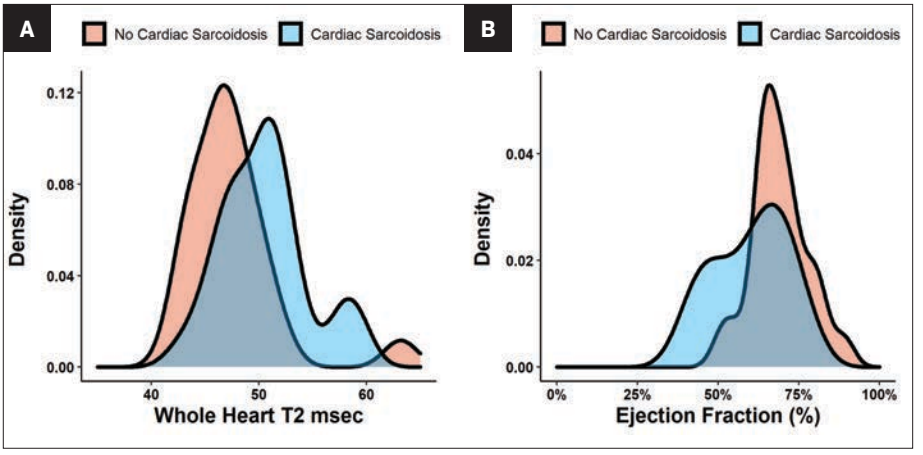

Cardiac Magnetic Resonance Imaging and T2 Mapping Parameters

All MRI studies were conducted on a 1.5T system (MAGNETOM Avanto, Siemens Healthineers, Erlangen, Germany). Cine acquisitions, native T2 mapping, and LGE imaging were performed as part of a comprehensive clinical cardiac MRI protocol. All subjects were scanned in a head-first supine position using 24-element spine and 6-element surface phased-array coils. All acquisitions were ECG triggered or gated and performed during end expiration. Native T2 mapping was performed in three short-axis slices (basal, midventricular and apical), using a commercially available T2 prepared bSSFP sequence with three preparation pulses of 0.0ms, 30.0ms and 55.0ms and a recovery period of three heart beats to obtain T2 maps in the diastolic phase. Further typical pulse sequence parameters were applied as follows: TR/TE 2.49 / 1.06 ms; FOV 360 × 210 mm; matrix 256 × 256;

Table 2. Summary values for cardiac function and segmental T2 values as stratified by diagnosis of cardiac sarcoidosis by CMR impression.

N = 55	CARDIAC SARCOIDOSIS (N = 32)		NO CARDIAC SARCOIDOSIS (N = 23)		
	Median	**IQR**	**Median**	**IQR**	**P**
SV	78	29.2	77	19	0.970
SVi	38.5	11.8	37	11	0.820
EDV	137.5	66.8	117	29	0.058
EDVi	63.5	29.2	57	19	0.038
ESV	56	31.2	39	14	0.002
ESVi	27	20	17	9	0.001
Ejection Fraction	62	18	68	9	0.009
Whole Heart T2	50.6	4.5	47.0	4.1	0.003
Average Basal T2	48.9	5.2	46.3	3.9	0.009
Average Mid T2	51.0	4.4	47.1	4.6	0.002
Average Apex T2	51.4	5.8	47.9	4.8	0.021
Average Septal T2	49.5	4.3	46.9	3.9	0.007
Average Inferior T2	50.4	4.6	46.3	5.1	0.002

SV = stroke volume, SVi = stroke volume (indexed). EDV = End diastolic volume, EDVi = End diastolic volume (indexed), ESV = End systolic volume, ESVi = End systolic volume (indexed). IQR = Interquartile range.

Figure 2. Distribution of T2 values by AHA left ventricular mapping segments and stratified by cardiac sarcoidosis.

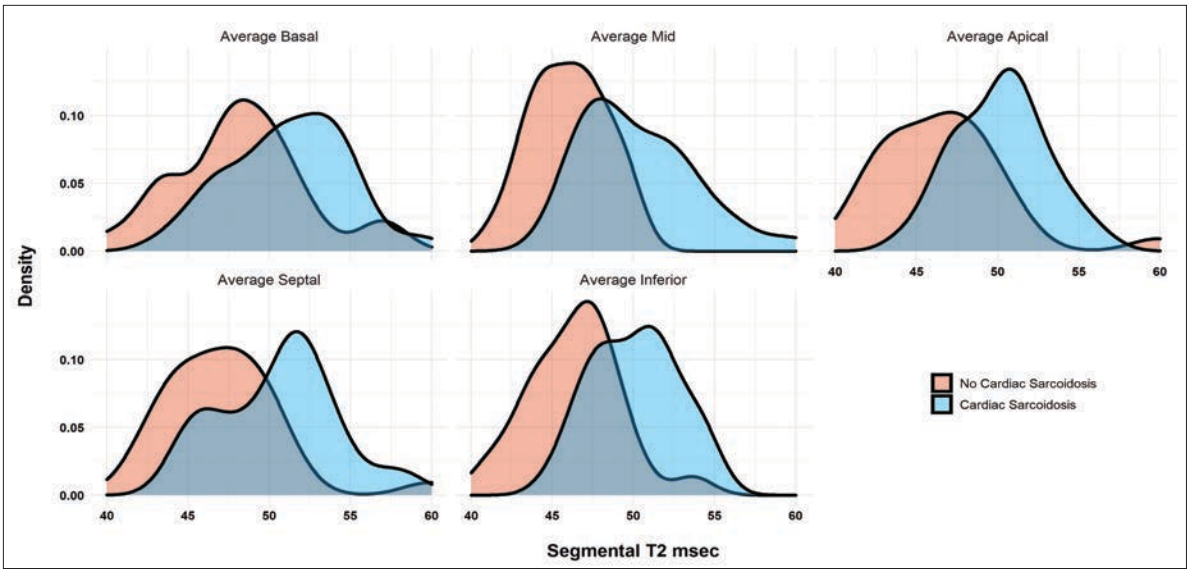

slice thickness 8 mm; flip angle 70°; and band width 1150 Hz/pixel.

Left Ventricular Segmentation

The left ventricle was divided into sixteen segments according to the AHA left ventricular mapping criteria.[17] Segment 17 was excluded due to inaccuracies in measurement in this region due to chest wall proximity. All segmentation was performed by one reader.

Statistical Analysis

A pretest power analysis was conducted for the pairwise comparison of T2 and cardiac function values between patients with and without cardiac sarcoidosis. Assuming a standard alpha of 0.05 and power of 0.8, effect sizes greater than or equal to 0.68 were reliably identified. For correlation of T2 and cardiac function values, correlations with a magnitude greater than 0.36 were reliably detected. Data was summarized using medians

Figure 3. Distribution of cardiac volume measurements stratified by cardiac sarcoidosis.

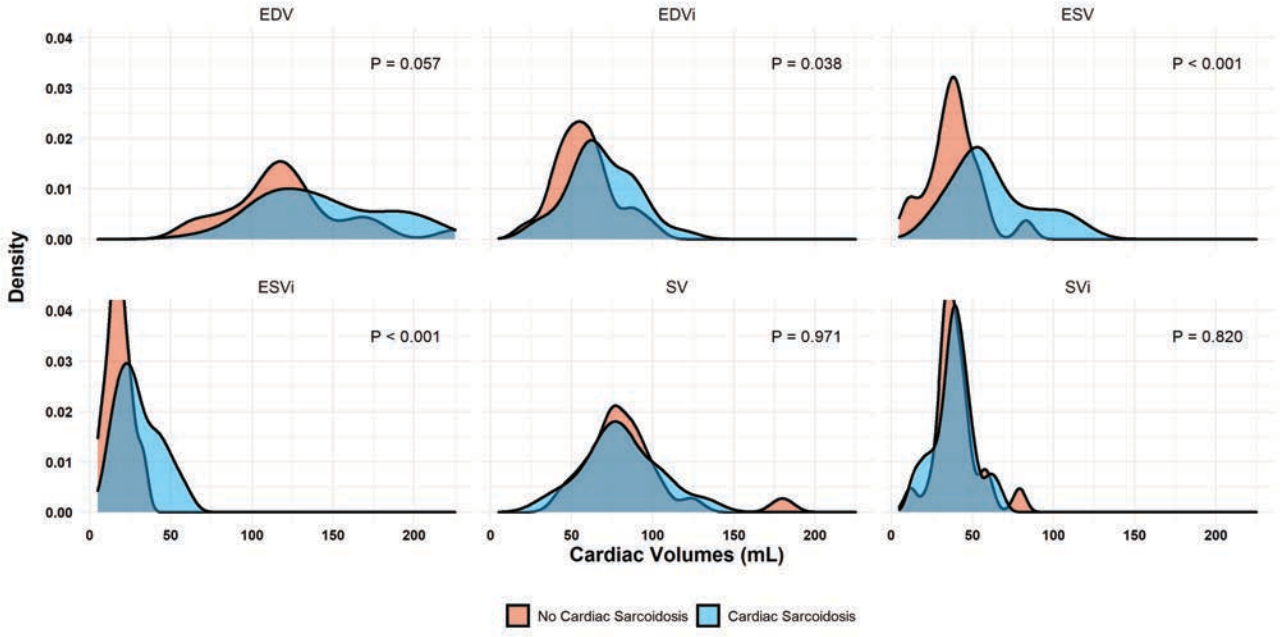

and interquartile ranges given the non-parametric distribution of data. Quantitative comparisons were conducted using the Mann-Whitney U test. Correlation analyses were performed using spearman's log-rank correlation.

Results

Fifty-five patients (32 with CS according to the WASOG criteria and 23 without) were included in the final cohort. (Table 1). Patients with CS had globally elevated T2 mapping values in comparison to those without cardiac sarcoidosis ($T2_{Wholeheart}$ 50.6 ± 4.5 vs 47.0 ± 4.1; p = 0.003). (Figure 1A). The segments with the highest T2 values were the apical and mid-ventricular segments (Median 51.4 and 51.0, respectively). The region with the most variability was also the apical segment (IQR 5.8). All segment T2 values were elevated in patients with CS as opposed to those without. (Table 2 and Figure 2).

Regarding cardiac function, patients with cardiac sarcoidosis had an average ejection fraction of 62 ± 18 vs 68 ± 9 (p = 0.009). (Figure 1B). Patients with CS also had elevated end-systolic volumes indexed to body mass index (BMI) (ESVi) compared to those without CS (27 ± 20 vs 17 ± 9; p = 0.002). Patients with CS also had higher end-diastolic volumes indexed to body mass index (EDVi) compared to those without CS (63.5 ± 29 vs 57 ± 19, p = 0.038), but nonindexed values were not significantly different (p = 0.058).

There was no difference in stroke volume between patients with and without CS (78 ± 29 vs 77 ± 19). (Table 2 and Figure 3). The normative values for patients with and without CS as stratified by ejection fraction is given in Table 3. Median T2 values for patients without CS ranged from 46.3 – 47.9. Patients without sarcoidosis but with ejection fractions of less than 55% ranged from 46.2 – 47.1%. The 75th percentile whole heart T2 value for patients without CS was 50.4. The median whole heart T2 value for patients with CS was 50.5 (IQR 5.2). The highest values for CS patients were observed in the apical and mid-ventricular segments (51.6 and 51.5, respectively). As a group, CS patients with normal and abnormal ejection fractions did not vary widely.

For segmental T2-functional measurement correlation, no regional T2 value was associated with increased EDVi. (Figure 4A). Correlations observed for EDVi ranged from -0.16 to +0.12. All segmental T2 measurements observed a positive correlation with ESVi; however, only the average mid-ventricular and average apical segments (R = 0.31 and 0.31; p = 0.032 and 0.039) were significant. Septal T2 values had a correlation coefficient of 0.25 but were not significantly correlated with ESVi. (Figure 4B).

Table 3. Segmental T2 values for patients stratified by reduced vs normal ejection fraction and cardiac sarcoidosis.

	CARDIAC SARCOIDOSIS			
	Ejection Fraction < 55%		Ejection Fraction > 55%	
	N = 11		N = 21	
T2/msec	**Median**	**IQR**	**Median**	**IQR**
Whole Heart	50.5	5.2	50.6	3.8
Average Basal	47.3	4.6	49.7	5.0
Average Mid	51.5	5.4	50.7	4.2
Average Apex	51.6	6.8	51.2	5.0
Average Septal	48.1	4.5	49.6	4.5
Average Inferior	50.5	5.0	50.4	3.2
	NO CARDIAC SARCOIDOSIS			
	Ejection Fraction < 55%		Ejection Fraction > 55%	
	N = 2		N = 21	
T2/msec	**Median**	**IQR**	**Median**	**IQR**
Whole Heart	46.7	—	47.0	3.4
Average Basal	46.2	—	46.3	4.2
Average Mid	47.0	—	47.1	4.4
Average Apex	47.1	—	47.9	4.0
Average Septal	46.9	—	46.9	3.1
Average Inferior	46.5	—	46.3	4.6
	ALL PATIENTS			
	Ejection Fraction < 55%		Ejection Fraction > 55%	
	N = 13		N = 42	
T2/msec	**Median**	**IQR**	**Median**	**IQR**
Whole Heart	49.3	5.6	48.7	5.1
Average Basal	47.3	3.7	48.1	4.9
Average Mid	49.8	5.9	48.6	5.4
Average Apex	50.9	7.3	50.1	6.2
Average Septal	48.1	4.5	48.3	5.1
Average Inferior	49.7	4.9	48.5	5.2

IQR = Interquartile range

Patients were divided into sub-analyses by classification of ejection fraction. A normal ejection fraction was defined as > 55%, the MRI-estimated threshold for abnormality. Patients with a normal ejection fraction only demonstrated correlation with average apical T2 values with a moderately negative relationship ($R = -0.37$, $p = 0.025$). In patients with reduced ejection fractions (< 55%), all T2 measurements were highly associated with decreased ejection fraction. Correlations ranged from -0.64 to -0.78. The highest correlated measurements were the inferior ($R = 0.78$, $p = 0.035$) and the apical ($R = -0.72$, $p = -0.013$) segments. The lowest ejection fraction in this cohort was measured at 38%. (Figure 5).

Discussion

The purpose of this study was to contribute normative segmental T2 values and the association of these medians with important MRI-derived cardiac function measurements in a sequential cohort of sarcoidosis patients. Patients with cardiac sarcoidosis as defined by WASOG criteria had elevated global and segmental T2 mapping values, decreased systolic function, and decreased ejection fraction as compared to patients without cardiac sarcoidosis. Median T2 values for CS patients were roughly found to be > 50 msec. Median values for patients without CS ranged from 46-47 msec. Elevated apical and mid-ventricular T2 values were associated with increased end-systolic volumes indexed to BMI and all T2 mapping values were highly negatively correlated with worsening ejection fraction in patients with heart failure with reduced ejection fraction. The T2 values of the inferior segments most highly correlated with worsening ejection fraction, but all measured segments were associated with varying degrees of dysfunction..

To date most studies regarding T2 mapping in CS have focused on either whole-heart or threshold T2 values and information regarding the regional variation of disease is lacking. Previous literature dating back to 2017 found that patients with CS had a median 3T whole-heart T2 value of 54 msec versus normal patients with 47 msec. Although 54 was higher than any of the median measurements in this study for patients with CS, it is within the interquartile range for both studies. The study cutoff for CS was found to be 47 msec, which is lower than the median reported in this study. This may be because the control patients in the previous

Figure 4. Correlation of BMI-indexed cardiac function measurements with T2 values. (A) T2 values were not significantly associated with changes in end diastolic volumes. (B) Apical and middle segment T2 values were moderately positively associated with increased end systolic volumes (R = 0.31 and 0.31).

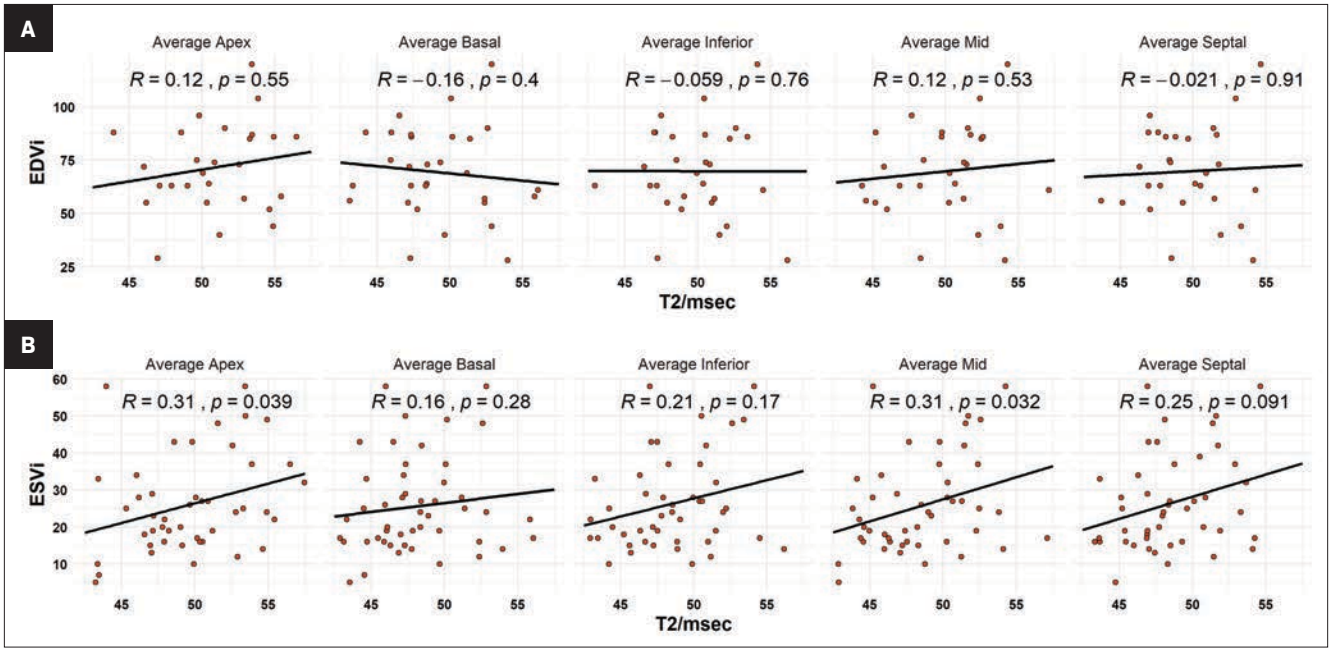

Figure 5. Correlation of T2 segment values with ejection fraction. (A) Patients with normal ejection fraction as measured by MRI-derived estimates (Normal > 55%). Apical T2 values were moderately negatively correlated with ejection fraction in patients with radiologically normal function (R = -0.37, p = 0.025). (B) Patients with reduced ejection fraction (< 55% by MRI-derived estimates).

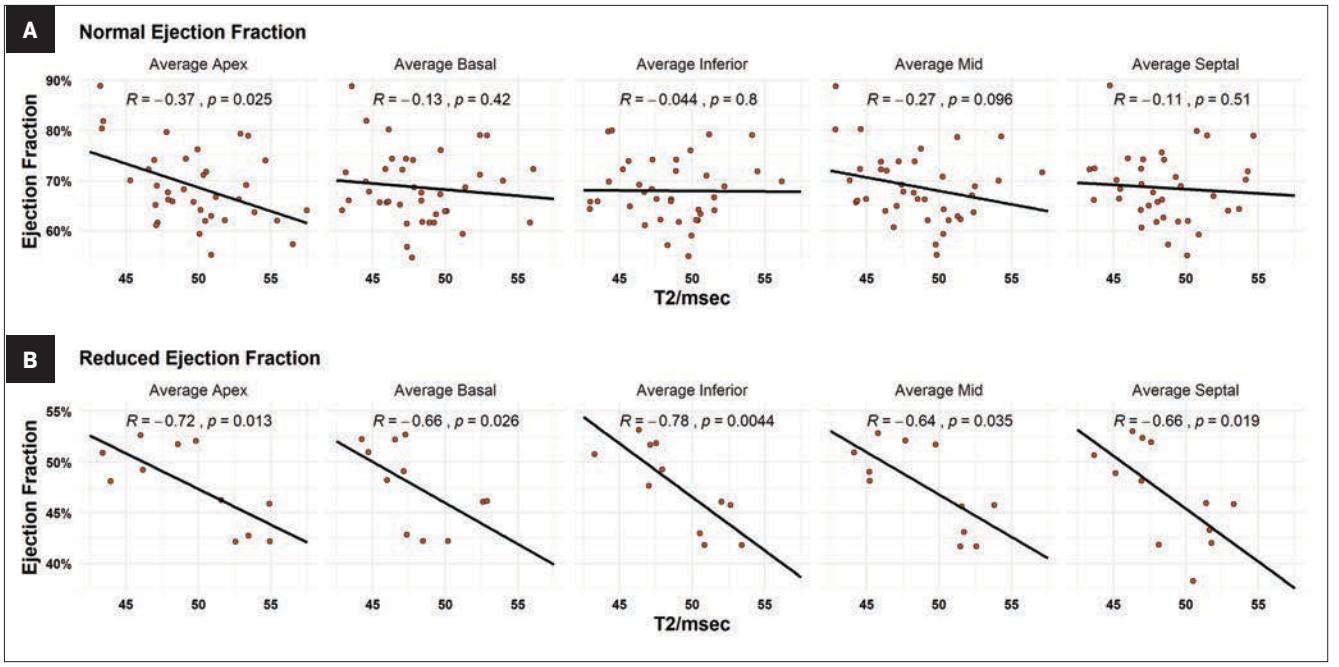

study were normal subjects with ostensibly normal hearts, while the control patients in this study represent older patients with baseline systemic sarcoidosis or because of the MRI field strength. A recent meta-analysis further suggested a median value of 52.6 msec for CS, once again within range of results.[14,19] Normative values may even vary due to segmentation methods (CS 50-54 T2msec) as demonstrated by Dabir, et al.[12] Lastly, a study of PET/MRI with T2 mapping found CS values to average 46 ± 5 msec, which is lower than previously published findings and likely related to their local parameters as mentioned in their methodology.

Recently, a previous meta-analysis summarized that CMR has a higher sensitivity for CS than PET/CT, but there is a remaining role for FDG-PET in the diagnosis of active disease.[2] T2 mapping as a measurement of myocardial edema has been postulated to fill this role and potentiate CMR as a complete study for diagnosis of chronic and active disease.[3] There is a distinct need for normative values indexed to AHA segments, as CS is well noted to have a predilection for the basal-, mid-, and inferior-left ventricular segments, and basal septal involvement is thought to lead to conduction system abnormalities.[1,20,21] The role of regional segmental T2 variation in systolic dysfunction is a new addition to the literature, with this study suggesting that the mid-inferior segments to be the most relevant. This correlates well with previous literate demonstrating LGE correlates with worsening LVEF.[22] Given the criteria for consideration of implantable defibrillation devices begins at an uncorrectable ejection fraction of 35%, the active phase edema represented by T2 may be an early warning for clinicians to pursue preventative therapies.[23]

The most controversial question regarding CS diagnosis must be the specific diagnostic criteria. Three criteria that have been put forth are those of the Japanese Circulation Society (JCS), the Heart Rhythm Society (HRS), and the World Association of Sarcoidosis and Other Granulomatous Disease (WASOG). Each takes a different approach: the JCS criteria use a major and minor criterion system, and the WASOG and HRS differ slightly regarding inclusion of perfusion imaging and T2 signal.[18,23,24] The authors of this study chose to utilize the WASOG criteria modified without the T2 signal to represent a diagnosis of CS. The authors chose the WASOG without T2 criteria in order to not create a circuitous diagnostic criterion and to reduce bias favoring CMR from JCS criteria (FDG-PET and LGE being major criteria), given that all patients in this study received CMR.

Additionally, given that endomyocardial biopsy is as low as 20% sensitivity for CS, the authors also note that "at least probable" per WASOG criteria is regarded as usually sufficient to diagnose CS.[18,25] Finally, the prevalence of CS in this study was 58%, which is higher than previously documented cohorts. The authors note the prevalence of CS in patients with symptomatic sarcoidosis to be 39% in recent analyses and this study likely includes selection bias owing to the patient population already having a high suspicion of disease.[26]

Novel implications of this study include the redemonstration of normative T2 mapping values for CS in the low 50s with additional description of regional variation. Additionally, regional T2 values are found to highly correlate with decreased ejection fraction and increased end-systolic volumes in patients with CS, especially those with < 55% EF. Limitations of this study include the lack of tissue-based criteria in WASOG definition and this cohort, the prior noted selection bias in who received a CMR, and the poor evaluation of diastolic dysfunction on CMR with the methods used. Further study should include multiple comparisons of different criteria in an expanded dataset and consider further evaluation of diastolic function.

Conclusions

Normative median segmental left ventricular T2 values in cardiac sarcoidosis range approximately from 49 to 51 msec. T2 values in the mid-apical region correlate with increased end-systolic volumes indexed to BMI. All segmental T2 values strongly correlate with decreasing ejection fraction in patients with ejection fraction of less than 55%.

References

1) Ribeiro Neto ML, Jellis CL, Joyce E, Callahan TD, Hachamovitch R, Culver DA. Update in cardiac sarcoidosis. *Ann Am Thorac Soc*. Nov 2019;16(11):1341-1350. doi:10.1513/AnnalsATS.201902-119CME

2) Aitken M, Chan MV, Urzua Fresno C, et al. Diagnostic accuracy of cardiac MRI versus FDG PET for cardiac sarcoidosis: a systematic review and meta-analysis. *Radiology*. May 17 2022:213170. doi:10.1148/radiol.213170

3) Cheung E, Ahmad S, Aitken M, et al. Combined simultaneous FDG-PET/MRI with T1 and T2 mapping as an imaging biomarker for the diagnosis and prognosis of suspected cardiac sarcoidosis. *Eur J Hybrid Imaging*. Dec 16 2021;5(1):24. doi:10.1186/s41824-021-00119-w

4) Skali H, Schulman AR, Dorbala S. 18F-FDG PET/CT for the assessment of myocardial sarcoidosis. *Curr Cardiol Rep*. Apr 2013;15(4):352.

5) Yoshida A, Ishibashi-Ueda H, Yamada N, et al. Direct comparison of the diagnostic capability of cardiac magnetic resonance and endomyocardial biopsy in patients with heart failure. *Eur J Heart Fail*. Feb 2013;15(2):166-75. doi:10.1093/eurjhf/hfs206

6) Davenport MS, Perazella MA, Yee J, et al. Use of intravenous iodinated contrast media in patients with kidney disease: consensus statements from the american college of radiology and the national kidney foundation. *Radiology*. Mar 2020;294(3):660-668. doi:10.1148/radiol.2019192094

7) Bakker AL, Grutters JC, Keijsers RG, Post MC. Cardiac sarcoidosis: challenges in clinical practice. *Curr Opin Pulm Med*. Sep 2017;23(5):468-475. doi:10.1097/MCP.0000000000000410

8) Smedema JP, Ainslie G, Crijns H. Review: Contrast-enhanced magnetic resonance in the diagnosis and management of cardiac sarcoidosis. *Prog Cardiovasc Dis*. May - Jun 2020;63(3):271-307. doi:10.1016/j.pcad.2020.03.011

9) Serei VD, Fyfe B. The many faces of cardiac sarcoidosis. *Am J Clin Pathol*. Feb 8 2020;153(3):294-302. doi:10.1093/ajcp/aqz169

10) Tana C, Mantini C, Donatiello I, et al. Clinical features and diagnosis of cardiac sarcoidosis. *J Clin Med*. May 1 2021;10(9) doi:10.3390/jcm10091941

11) Puntmann VO, Isted A, Hinojar R, Foote L, Carr-White G, Nagel E. T1 and T2 mapping in recognition of early cardiac involvement in systemic sarcoidosis. *Radiology*. Oct 2017;285(1):63-72. doi:10.1148/radiol.2017162732

12) Dabir D, Luetkens J, Kuetting D, Nadal J, Schild HH, Thomas D. Myocardial mapping in systemic sarcoidosis: a comparison of two measurement approaches. *Rofo*. Jan 2021;193(1):68-76. Myokardiales mapping bei systemischer sarkoidose: ein vergleich zweier messansatze. doi:10.1055/a-1174-0537

13) Crouser ED, Ono C, Tran T, He X, Raman SV. Improved detection of cardiac sarcoidosis using magnetic resonance with myocardial T2 mapping. *Am J Respir Crit Care Med*. Jan 1 2014;189(1):109-12. doi:10.1164/rccm.201309-1668LE

14) Snel GJH, van den Boomen M, Hernandez LM, et al. Cardiovascular magnetic resonance native T2 and T2(*) quantitative values for cardiomyopathies and heart transplantations: a systematic review and meta-analysis. *J Cardiovasc Magn Reson*. May 11 2020;22(1):34. doi:10.1186/s12968-020-00627-x

15) Crouser ED, Ruden E, Julian MW, Raman SV. Resolution of abnormal cardiac MRI T2 signal following immune suppression for cardiac sarcoidosis. *J Investig Med*. Aug 2016;64(6):1148-50. doi:10.1136/jim-2016-000144

16) Schulz-Menger J, Wassmuth R, Abdel-Aty H, et al. Patterns of myocardial inflammation and scarring in sarcoidosis as assessed by cardiovascular magnetic resonance. *Heart*. Mar 2006;92(3):399-400. doi:10.1136/hrt.2004.058016

17) Cerqueira MD, Weissman NJ, Dilsizian V, et al. Standardized myocardial segmentation and nomenclature for tomographic imaging of the heart. A statement for healthcare professionals from the Cardiac Imaging Committee of the Council on Clinical Cardiology of the American Heart Association. *Circulation*. Jan 29 2002;105(4):539-42. doi:10.1161/hc0402.102975

18) Judson MA, Costabel U, Drent M, et al. The WASOG sarcoidosis organ assessment instrument: an update of a previous clinical tool. *Sarcoidosis Vasc Diffuse Lung Dis*. Apr 18 2014;31(1):19-27.

19) reulich S, Gatidis S, Grani C, et al. Hybrid cardiac magnetic resonance/fluorodeoxyglucose positron emission tomography to differentiate active from chronic cardiac sarcoidosis. *JACC Cardiovasc Imaging*. Mar 2022;15(3):445-456. doi:10.1016/j.jcmg.2021.08.018

20) Patel MR, Cawley PJ, Heitner JF, et al. Detection of myocardial damage in patients with sarcoidosis. *Circulation*. Nov 17 2009;120(20):1969-77. doi:10.1161/CIRCULATIONAHA.109.851352

21) Kouranos V, Tzelepis GE, Rapti A, et al. Complementary role of cmr to conventional screening in the diagnosis and prognosis of cardiac sarcoidosis. *JACC Cardiovasc Imaging*. Dec 2017;10(12):1437-1447. doi:10.1016/j.jcmg.2016.11.019

22) Watanabe E, Kimura F, Nakajima T, et al. Late gadolinium enhancement in cardiac sarcoidosis: characteristic magnetic resonance findings and relationship with left ventricular function. *J Thorac Imaging*. Jan 2013;28(1):60-6. doi:10.1097/RTI.0b013e3182761830

23) Birnie DH, Sauer WH, Bogun F, et al. HRS expert consensus statement on the diagnosis and management of arrhythmias associated with cardiac sarcoidosis. *Heart Rhythm*. Jul 2014;11(7):1305-23. doi:10.1016/j.hrthm.2014.03.043

24) Terasaki F, Azuma A, Anzai T, et al. JCS 2016 guideline on diagnosis and treatment of cardiac sarcoidosis- digest version. *Circ J*. Oct 25 2019;83(11):2329-2388. doi:10.1253/circj.CJ-19-0508

25) Vignaux O. Cardiac sarcoidosis: spectrum of MRI features. *AJR Am J Roentgenol*. Jan 2005;184(1):249-54. doi:10.2214/ajr.184.1.01840249

26) Martusewicz-Boros MM, Boros PW, Wiatr E, Zych J, Piotrowska-Kownacka D, Roszkowski-Sliz K. Prevalence of cardiac sarcoidosis in white population: a case-control study: Proposal for a novel risk index based on commonly available tests. *Medicine (Baltimore)*. Aug 2016;95(32):e4518. doi:10.1097/MD.0000000000004518

Review of Clinically Significant Cancer in Lesions Labeled PI-RADS 3 on MRI Using PI-RADS Version 2.1

Alexander M. Satei MBBS[1,2], Mehrvaan Kaur MBBS[1,2], Jeffrey MacLean MD[1,2], Bashir Hakim MD[1,2,3]

Abstract

Objective and Hypothesis: Prostate Imaging Reporting and Data System (PI-RADS) category 3 represents an intermediate risk of clinically significant prostate cancer. These lesions are detected on magnetic resonance (MRI) using a combination of T2, DWI/ADC, and DCE sequences. Besides being labeled as equivocal, there is no definitively stated percent risk of clinically significant cancer for these lesions. This article reviewed literature surrounding PI-RADS version 2.1 category 3 prostate lesions on MRI.

Methods: The PubMed database was searched on October 4, 2022. Articles included in this review included only the newest version of PI-RADS, version 2.1, which was released in 2019. Primary endpoints included the incidence of prostate cancer and clinically significant prostate cancer.

Results: Eleven studies were included in this review, encompassing 1,481 PI-RADS 3 lesions exclusively evaluated using PI-RADS version 2.1. Clinically significant cancer was only found in 11.1% (n=164) of these lesions. The overall incidence of prostate cancer within these lesions was 21.4% (n=253), of the 1,185 PI-RADS 3 lesions included in this portion of the review.

Conclusion: The risk of clinically significant prostate cancer in PI-RADS 3 lesions evaluated using PI-RADS version 2.1 is low. However, individual patient factors, including age, previous biopsy status, prostate health index, and prostate specific antigen density should be considered when determining appropriateness of biopsy. Further research, including longitudinal studies involving future risk of clinically significant cancer in PI-RADS 3 lesions, would be beneficial for evaluation of the newest update of this increasingly popular reporting system.

Key words: PI-RADS, magnetic resonance imaging, prostate, prostate cancer, clinically significant cancer, structured reporting.

Introduction

The Prostate Imaging Reporting and Data System (PI-RADS) represents a standard for the reporting of prostate lesions on magnetic resonance imaging (MRI). Initially published by the American College of Radiology (ACR) in late 2011, a second edition (v2.0) was released in 2017, which was further updated in 2019 and titled version 2.1 (v2.1). PI-RADS has since gained popularity among radiologists and hospital systems as a standardized reporting system for interpreting and dictating prostate MRI cases. These categories, ranging from PI-RADS 1 to PI-RADS 5, help give clinicians a better understanding of the risk a prostatic lesion carries for clinically significant cancer. Table 1 summarizes the most recent update of the risk of clinically significant prostate cancer, adapted from the ACR's PI-RADS v2.1.[1]

An interesting conundrum arises from PI-RADS 3 lesions. Due to

Affiliations: [1]Department of Radiology, Trinity Health Oakland Hospital, Pontiac, Michigan; [2]Department of Radiology, Wayne State University School of Medicine, Detroit, Michigan; [3]Department of Radiology, Huron Valley Radiology, Ypsilanti, Michigan
Conflict of interest and support statement: The authors declare no competing interests and received no funding or external support for this work.
Prior publication/presentation: No prior publication of this data has occurred.
Data availability statement: Data sharing is not applicable as no datasets were generated/analyzed for this study.

the ambiguity of the intermediate risk classification, management of these lesions can vary widely. The ACR specifically states, "for findings with PI-RADS Assessment Category 3, biopsy may or may not be appropriate".[1] Typically, in cases of PI-RADS 3 lesions, clinicians will correlate imaging findings with other patient factors, including age, prostate-specific antigen (PSA) level, digital rectal exam results, and individual patient history.

While each PI-RADS category carries a general descriptive risk of clinically significant prostate cancer, it does not provide a quantifiable risk of prostate cancer. Additionally, there are no definitive guidelines for management provided by the ACR based on the PI-RADS categorization. In reality, PI-RADS 1 and PI-RADS 2 lesions are managed conservatively as if they are benign, while PI-RADS 4 and PI-RADS 5 lesions are treated with biopsy and excision as if they are malignant.

PI-RADS v2.1 updates how each category is interpreted. One significant change includes the potential to upgrade transition zone lesions initially scored as PI-RADS 2 by T2 imaging (T2I) into category 3 lesions if diffusion weighted imaging (DWI) corresponds to a score ≥ 4.[2] Additional descriptive criteria for PI-RADS 3 lesions, including specifying that the lesion needs to be "discrete and different from the background" as well as the use of the term "marked" to describe apparent diffusion coefficient (ADC) and DWI lesion intensities, have been added.[2]

The new changes in v2.1 were enacted to help overcome the limitations of v2.0. However, v2.1 continues to use the rather vague intermediate/equivocal characterization of PI-RADS 3 lesions, without providing a definitive risk for clinically significant cancer. Review articles exploring the risk of clinically significant cancer in v2.0 noted such cancer in approximately 16-21% of biopsied PI-RADS 3 lesions, with variation depending on the patient's prior biopsy and cancer history.[3]

Table 1. Summary of the risk of clinically significant prostate cancer stratified by PI-RADS category, adapted from ACR PI-RADS v2.1 guidelines.

PI-RADS CATEGORY	RISK OF CLINICALLY SIGNIFICANT CANCER
1	Very low / Highly unlikely
2	Low / Unlikely
3	Intermediate / Equivocal
4	High / Likely
5	Very high / Highly likely

With the previously mentioned changes to PI-RADS version 2.1, further research is required to clarify intermediate risk of prostate cancer in PI-RADS category 3 lesions. This article seeks to determine the risk of clinically significant cancer in PI-RADS 3 lesions through a review of literature. We hypothesize that the changes incorporated into PI-RADS version 2.1 will not significantly alter the incidence of clinically significant cancer diagnosed from lesions labeled as PI-RADS 3.

Methods and Materials

We conducted a literature search utilizing PubMed to find articles in the English language that include biopsy results of PI-RADS 3 lesions, using the term "PI-RADS 3". The time frame included was 2017-2019. This time frame is appropriate as it includes only v2.1 of PI-RADS onward. Exclusion criteria included inappropriate study design; ie, case report, review articles, etc; an incorrect version of PI-RADS (only studies involving PI-RADS v2.1 were included), and published in non-English-language journals.

A total of 11 full-length articles were included in the final review. They were analyzed for the number of PI-RADS 3 lesions and the frequency of prostate cancer (PCa) and clinically significant prostate cancer (cs-PCa). The findings are summarized in Table 2.

Results

In our literature search, PI-RADS 3 lesions did not constitute a significant number of MRI results, with the majority of lesions being labeled PI-RADS categories 1 or 2. The number and countries of origin of included studies were the United States (4), China (3), Germany (2), Canada (1), and Italy (1). The range of median age for the participants in the included studies was 59.0-69.3.

In total, 1481 PI-RADS 3 lesions were included in the current review, of which 164 (11.1%) contained clinically significant cancer. The range of clinically significant prostate cancer in the current review article was relatively wide, with a frequency of 4.5-27.2% of PI-RADS 3 lesions; however, most of the studies suggested a frequency of less than 10%.

Of the 1185 lesions described in articles that provided information about the frequency of prostate cancer, 21.4% were cancerous (n=253). These included both clinically insignificant and clinically significant prostate cancers.

Table 2. Summary of studies included in the current review article.[4-14]

AUTHOR	YEAR	COUNTRY	MEDIAN AGE	PI-RADS 3 LESIONS (N)	PCA (N, %)	CS-PCA LESIONS (N, %)
Rudolph[4]	2020	Germany	66.8	56	—	6 (10.7%)
Costa[5]	2021	US	65.4	110	17 (15.5%)	10 (9.1%)
Natale[6]	2021	US	68.2	230	31 (13.5%)	18 (7.8%)
Hectors[7]	2021	US	64.2	240	—	28 (11.7%)
Lim[8]	2021	Canada	64.8	95	36 (37.9%)	14 (14.7%)
Giambelluca[9]	2021	Italy	65.0	46	19 (41.3%)	7 (15.2%)
Wang[10]	2021	China	69.3	333	66 (19.8%)	33 (9.9%)
Arcot[11]	2022	US	66.0	90	22 (24.4%)	8 (8.8%)
Boschheidgen[12]	2022	Germany	59.0	89	19 (21.3%)	4 (4.5%)
Wei[13]	2022	China	66.7	89	10 (11.2%)	8 (9.0%)
Jin[14]	2022	China	67.5	103	33 (32.0%)	28 (27.2%)

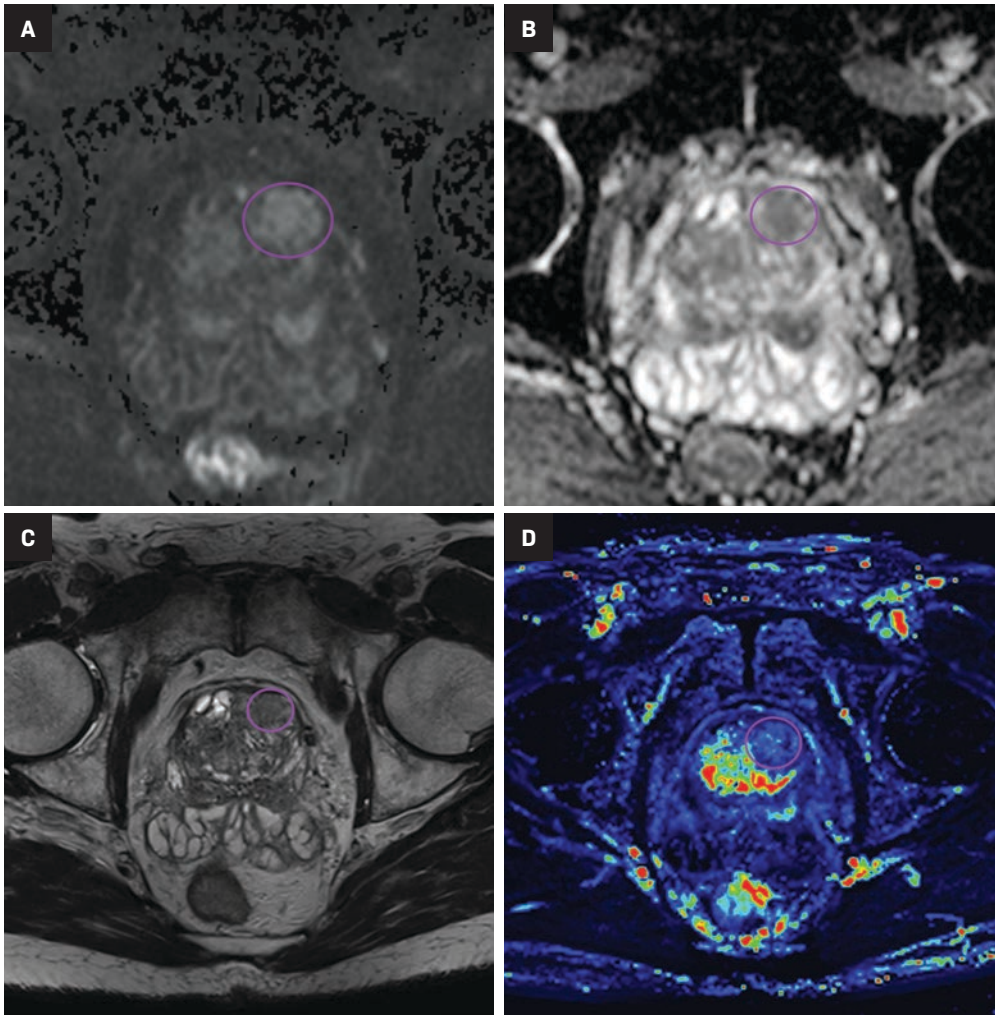

Figure 1. Example of a peripheral zone PI-RADS 3 lesion. Lesion in the left anterior peripheral zone of the prostate base which shows subtle hyperintensity on high-b value DWI (A), subtle hypointensity on the ADC map (B), noncircumscribed, rounded, moderate hypointensity on T2WI (C), and color maps showing the lesion is negative for DCE (D).

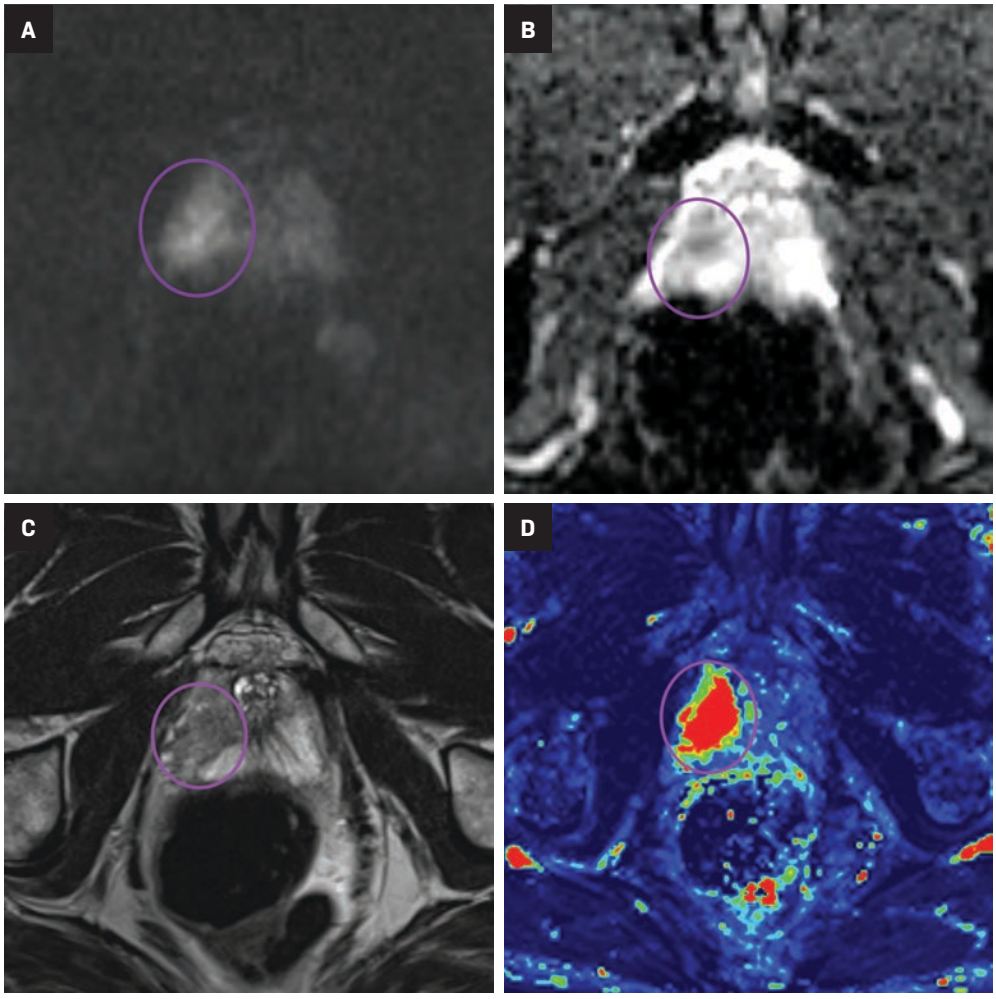

Figure 2. Example of a peripheral zone lesion upgraded from PI-RADS 3 to PI-RADS 4 based on DCE. Lesion in the right posterior peripheral zone of the prostate which shows subtle hyperintensity on high-b value DWI (A), hypointensity on the ADC map (B), mild heterogeneous hypointensity with obscured borders on T2WI (C), and color maps showing the lesion is positive for DCE (D).

A clear majority of PI-RADS 3 lesions were either benign or clinically insignificant cancer (n=1,317, 88.9%). Overall, the risk of clinically significant cancer for PI-RADS 3 lesions in our review was low.

Discussion

Defining PI-RADS 3

Prostate lesions are assigned a PI-RADS category based on their appearance on T2I, DWI/ADC, and dynamic contrast-enhanced (DCE) sequences. Like all PI-RADS category imaging findings, PI-RADS 3 lesions vary in appearance based upon their location within the prostate gland.

Lesions within the peripheral zone utilize DWI/ADC as the dominant sequence for categorization. To be classified as a PI-RADS 3 lesion, a lesion must display "[f]ocal (discrete and different from the background) hypointense on ADC and/or focal hyperintense on high b-value DWI; may be markedly hypointense on ADC or markedly hyperintense on high b-value DWI, but not both."1 PI-RADS v2.1 clarified that "marked" restriction refers to "a more pronounced signal change than any other focus in the same zone."[1] Figure 1 illustrates an example of a peripheral zone PI-RADS 3 lesion.

Additionally, to be categorized as PI-RADS 3, a lesion must be negative for DCE; ie, "no early or contemporaneous enhancement; or diffuse multifocal enhancement NOT corresponding to a focal finding on T2W and/or DWI or focal enhancement corresponding to a lesion demonstrating features of BPH on T2WI (including features of extruded BPH in the PZ)."[1] If the lesion is positive for DCE; ie, "focal, and; earlier than or contemporaneously with enhancement of adjacent normal prostatic tissues, and corresponds to suspicious finding on T2W and/or DWI", that lesion is upgraded to PI-RADS 4.[1] Figure 2 illustrates an example of a peripheral zone lesion upgraded from PI-RADS 3 to PI-RADS 4 based on positivity on DCE; this patient underwent prostatectomy, which showed prostatic adenocarcinoma with a Gleason Score of 9 (4+5).

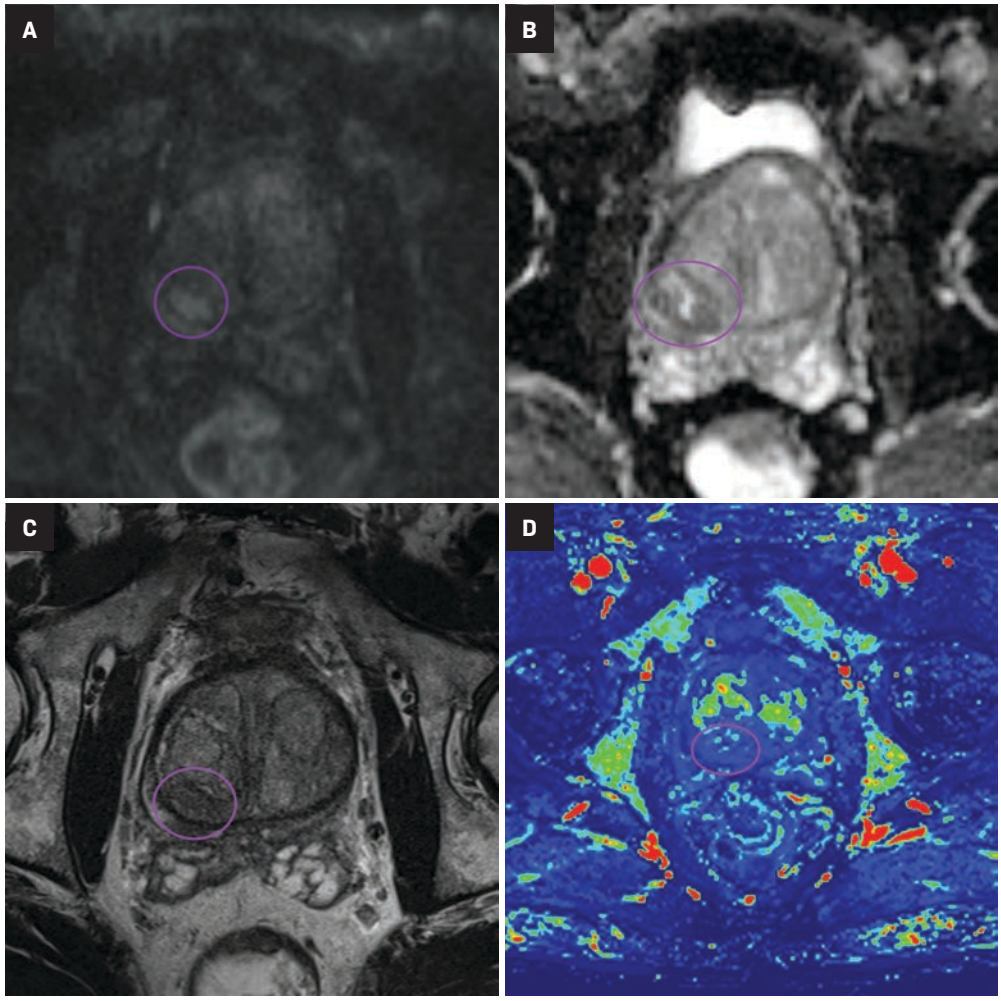

Figure 3. Example of a transitional zone PI-RADS 3 lesion. Lesion in the right posterior transition zone of the prostate which shows subtle hyperintensity on high-b value DWI (A), subtle hypointensity on the ADC map (B), mild heterogeneous hypointensity with obscured borders on T2I (C), and color maps showing the lesion is negative for DCE (D).

Lesions within the transitional zone utilize T2 as the dominant sequence. PI-RADS 3 is described as "[H]eterogeneous signal intensity or with obscured margins," as well as other lesions "that do not qualify as 2, 4, or 5".[1]

Similar to the peripheral zone, PI-RADS 3 lesions in the transitional zone can be recategorized based on additional imaging characteristics. Lesions which initially receive a score of PI-RADS 2 on T2I can be upgraded to PI-RADS 3 "if they have a DWI score greater than or equal to 4;" ie, if they have marked diffusion.[1] Lesions initially categorized as PI-RADS 3 can be upgraded to PI-RADS 4 "if they have a DWI score of 5;" ie, marked diffusion and greater than or equal to 1.5 cm in size).[1] Figure 3 illustrates an example of a transitional zone PI-RADS 3 lesion.

Despite the new forms of lesion categorization in v2.1, the limited number of studies comparing PI-RADS v2.0 to v2.1 have been mixed. Some studies have suggested v2.1 improves detection of transitional zone lesions, while others have shown no significant difference in the diagnostic performance between the two versions.[4,15,16] Issues remaining with PI-RADS v2.1 include the lack of a category for lesions that do not fit into the currently existing five categories and lack of standardization for the way background changes are evaluated.[17]

Defining Clinically Significant Prostate Cancer

There is no universal definition of clinically significant prostate cancer. However, within the PI-RADS system, clinically significant cancer is defined through pathologic examination of a lesion. PI-RADS defines a clinically significant lesion as one which contains any of the following[1]:

1. A Gleason score ≥ 7. This includes 3+4 lesions with prominent but not predominant Gleason 4 components.
2. Tumor volume totaling ≥ 0.5cc.
3. The presence of extraprostatic extension (EPE).

More recent literature may refer to the new Gleason scoring grades, where a score of 2 represents an old Gleason score of 3+4 (predominantly well-formed glands with a lesser component of poorly formed glands), while a score of 3 represents an old Gleason score of 4+3 (predominantly poorly formed glands with a lesser component of well-formed glands). This is to eliminate confusion as the latter represents more aggressive disease.[18] Using the new Gleason scoring system, a grade of 2 or more represents clinically significant disease.

Management of PI-RADS 3 Lesions

PI-RADS 3 lesions are difficult to manage, owing to their overlapping findings with benign conditions like prostatitis, benign prostatic hyperplasia and fibrosis. Some tumors are smaller and infiltrative, which may further hinder the diagnosis.[3] A balance must be attained to lower overdiagnosis and not to miss clinically significant prostate cancer.

British NICE guidelines regarding prostate cancer are based on a 5-point Likert prostate scale, a similar standardized scoring tool that includes clinical parameters.[19] The 5-point Likert scale is considered equivalent to the 5-point PI-RADS scale. NICE guidelines recommend biopsy for lesions with a Likert score of 3 or more.[20] Meanwhile, the European Association of Urology guidelines, which rely on PI-RADS scoring, recommend biopsy for all PI-RADS 3 lesions.[21]

The ACR does not provide any management recommendations. It invariably depends on the discretion of the clinical team on how to proceed. Patient factors such as a patient's age, comorbidities, and treatment preferences, must be taken into account.

Contributory Factors to Clinically Significant Cancer

Only a handful of articles have been published under the latest version of PI-RADS assessing the relationship of clinical factors and clinically significant prostate cancer in PI-RADS 3 lesions.

The prostate-specific antigen (PSA) score is widely accepted as a marker for screening and management, and the relationship between PSA density (PSAD), calculated by dividing total PSA by prostate volume, and PI-RADS lesions has previously been investigated. One study assessed the role of elevated PSAD in transitional zone PI-RADS lesions, with elevated PSA ranging from 4-20 ng/ml. The evidence showed a higher prediction of clinically significant prostate cancer for PSAD levels greater than 0.15 ng/ml/ml.[6] Another study subclassified PI-RADS 3 lesions into 3a (lower-risk lesions with volume < 0.5 ml) and 3b (higher-risk lesions with volume ≥0.5 ml). They found a 100% sensitivity and positive predictive value in detecting clinically significant prostate cancer in patients in the 3b category with a PSAD greater than 0.15 ng/ml/ml.[22]

PSA-based tools such as the prostate health index (PHI) are also becoming more widely used. The PHI takes into account the [-2]proPSA and free PSA levels. A study evaluating the role of PHI in a group of 143 men evaluated using PI-RADS v2.0 found that PHI was useful for avoiding unnecessary biopsies.[23] In patients with PHI value of 49 and more, approximately 55% of biopsies could be avoided without missing clinically significant cancers.

Other factors, including older age and biopsy naive status, have been associated with clinically significant prostate cancer. In contrast, men with at least one negative biopsy were found to have a lower risk.[24] A retrospective study of 141 patients evaluated using PI-RADS v2.0 showed a mean interval of approximately 12.4 months to be optimal for follow-up MRI rather than immediate biopsy in PI-RADS 3 lesions.[25]

Limitations and Opportunities for Further Research

Limitations of this study primarily center around available data. This review only examines lesions classified by the most recent version of PI-RADS, with few studies utilizing this criteria undertaken since its debut in 2019. Additionally, within the available data some articles included in our review did not discriminate between lesions and patients. For example, a single patient may have multiple lesions, confounding their risk for clinically significant cancer.

As more data is collected and more research is conducted utilizing the PI-RADS v2.1 approach, sample sizes will become more robust, allowing for increased confidence in conclusions. Further longitudinal studies to allow for evaluation of PI-RADS 3 lesions over time would be beneficial in determining future risk for clinically significant cancer. Studies incorporating clinical tools such as PSAD, PHI, and patient history could evaluate the benefit for clinical teams to include this information in their decision-making process. Finally, additional research comparing v2.0 to v2.1 can help in the development of future PI-RADS versions by exposing the possible limitations of this continually developing reporting system.

Conclusion

The present literature review of 11 articles evaluating prostate

cancer and clinically significant prostate cancer using PI-RADS version 2.1 reveals low levels of clinically significant cancer. However, contributory individual patient factors such as age, PSAD, PHI, and biopsy status should be considered before deciding whether to perform diagnostic biopsy. As PI-RADS continues to gain popularity as a standardized reporting system for prostate lesions, continued research will be instrumental in the further evolution of the PI-RADS system.

References

1) ACR.org. PI-RADS prostate imaging – reporting and data system. 2019. Available at: <https://www.acr.org/-/media/ACR/Files/RADS/PI-RADS/PIRADS-V2-1.pdf> [Accessed 4 October 2022].

2) Purysko AS, Rosenkrantz AB, Turkbey IB, Macura KJ. Radiographics update: PI-RADS version 2.1-a pictorial update. Radiographics. 2020 Nov-Dec;40(7):E33-E37. doi: 10.1148/rg.2020190207

3) Schoots IG. MRI in early prostate cancer detection: how to manage indeterminate or equivocal PI-RADS 3 lesions? Transl Androl Urol. 2018 Feb;7(1):70-82. doi: 10.21037/tau.2017.12.31

4) Rudolph MM, Baur ADJ, Cash H, Haas M, Mahjoub S, Hartenstein A, Hamm CA, Beetz NL, Konietschke F, Hamm B, Asbach P, Penzkofer T. Diagnostic performance of PI-RADS version 2.1 compared to version 2.0 for detection of peripheral and transition zone prostate cancer. Sci Rep. 2020 Sep 29;10(1):15982. doi: 10.1038/s41598-020-72544-z

5) Costa DN, Jia L, Subramanian N, Xi Y, Rofsky NM, Recchimuzzi DZ, de Leon AD, Arraj P, Pedrosa I. Prospective PI-RADS v2.1 atypical benign prostatic hyperplasia nodules with marked restricted diffusion: detection of clinically significant prostate cancer on multiparametric MRI. AJR Am J Roentgenol. 2021 Aug;217(2):395-403. doi: 10.2214/AJR.20.24370

6) Natale C, Koller CR, Greenberg JW, Pincus J, Krane LS. Considering predictive factors in the diagnosis of clinically significant prostate cancer in patients with PI-RADS 3 lesions. Life (Basel). 2021 Dec 19;11(12):1432. doi: 10.3390/life11121432

7) Hectors SJ, Chen C, Chen J, Wang J, Gordon S, Yu M, Al Hussein Al Awamlh B, Sabuncu MR, Margolis DJA, Hu JC. Magnetic resonance imaging radiomics-based machine learning prediction of clinically significant prostate cancer in equivocal PI-RADS 3 lesions. J Magn Reson Imaging. 2021 Nov;54(5):1466-1473. doi: 10.1002/jmri.27692

8) Lim CS, Abreu-Gomez J, Carrion I, Schieda N. Prevalence of prostate cancer in PI-RADS version 2.1 transition zone atypical nodules upgraded by abnormal DWI: correlation with MRI-directed TRUS-guided targeted biopsy. AJR Am J Roentgenol. 2021 Mar;216(3):683-690. doi: 10.2214/AJR.20.23932

9) Giambelluca D, Cannella R, Vernuccio F, Comelli A, Pavone A, Salvaggio L, Galia M, Midiri M, Lagalla R, Salvaggio G. PI-RADS 3 lesions: role of prostate MRI texture analysis in the identification of prostate cancer. Curr Probl Diagn Radiol. 2021 Mar-Apr;50(2):175-185. doi: 10.1067/j.cpradiol.2019.10.009

10) Wang ZB, Wei CG, Zhang YY, Pan P, Dai GC, Tu J, Shen JK. The role of PSA density among PI-RADS v2.1 categories to avoid an unnecessary transition zone biopsy in patients with PSA 4-20 ng/mL. Biomed Res Int. 2021 Oct 11;2021:3995789. doi: 10.1155/2021/3995789

11) Arcot R, Sekar S, Kotamarti S, Krischak M, Michael ZD, Foo WC, Huang J, Polascik TJ, Gupta RT. Structured approach to resolving discordance between PI-RADS v2.1 score and targeted prostate biopsy results: an opportunity for quality improvement. Abdom Radiol (NY). 2022 Aug;47(8):2917-2927. doi: 10.1007/s00261-022-03562-w

12) Boschheidgen M, Schimmöller L, Doerfler S, Al-Monajjed R, Morawitz J, Ziayee F, Mally D, Quentin M, Arsov C, Albers P, Antoch G, Ullrich T. Single center analysis of an advisable control interval for follow-up of patients with PI-RADS category 3 in multiparametric MRI of the prostate. Sci Rep. 2022 Apr 25;12(1):6746. doi: 10.1038/s41598-022-10859-9

13) Wei X, Xu J, Zhong S, Zou J, Cheng Z, Ding Z, Zhou X. Diagnostic value of combining PI-RADS v2.1 with PSAD in clinically significant prostate cancer. Abdom Radiol (NY). 2022 Oct;47(10):3574-3582. doi: 10.1007/s00261-022-03592-4

14) Jin P, Yang L, Qiao X, Hu C, Hu C, Wang X, Bao J. Utility of clinical-radiomic model to identify clinically significant prostate cancer in biparametric MRI PI-RADS v2.1 category 3 lesions. Front Oncol. 2022 Feb 24;12:840786. doi: 10.3389/fonc.2022.840786

15) Wang Z, Zhao W, Shen J, Jiang Z, Yang S, Tan S, Zhang Y. PI-RADS version 2.1 scoring system is superior in detecting transition zone prostate cancer: a diagnostic study. Abdom Radiol (NY). 2020 Dec;45(12):4142-4149. doi: 10.1007/s00261-020-02724-y

16) Bhayana R, O'Shea A, Anderson MA, Bradley WR, Gottumukkala RV, Mojtahed A, Pierce TT, Harisinghani M. PI-RADS versions 2 and 2.1: interobserver agreement and diagnostic performance in peripheral and transition zone lesions among six radiologists. AJR Am J Roentgenol. 2021 Jul;217(1):141-151. doi: 10.2214/AJR.20.24199. Epub 2020 Sep 9. PMID: 32903060.

17) Purysko AS, Baroni RH, Giganti F, Costa D, Renard-Penna R, Kim CK, Raman SS. PI-RADS version 2.1: a critical review, from the AJR special series on radiology reporting and data systems. AJR Am J Roentgenol. 2021 Jan;216(1):20-32. doi: 10.2214/AJR.20.24495. Epub 2020 Nov 19. PMID: 32997518.

18) Epstein JI, Egevad L, Amin MB, Delahunt B, Srigley JR, Humphrey PA. The 2014 international society of urological pathology (ISUP) consensus conference on gleason grading of prostatic carcinoma: definition of grading patterns and proposal for a new grading system. Am J Surg Pathol. 2016 Feb;40(2):244-52. doi: 10.1097/PAS.0000000000000530

19) Latifoltojar A, Appayya MB, Barrett T, Punwani S. Similarities and differences between likert and PIRADS v2.1 scores of prostate multiparametric MRI: a pictorial review of histology-validated cases. Clin Radiol. 2019 Nov;74(11):895.e1-895.e15. doi: 10.1016/j.crad.2019.08.020

20) NICE.org.uk. Prostate cancer: diagnosis and management. Dec 2021. Available at: <https://www.nice.org.uk/guidance/ng131/chapter/Recommendations#assessment-and-diagnosis> [Accessed 4 October 2022].

21) Uroweb.org. Guidelines on prostate cancer. 2022. Available at: <https://uroweb.org/guidelines> [Accessed 4 October 2022].

22) Rico L, Blas L, Vitagliano G, Contreras P, Rios Pita H, Ameri C. PI-RADS 3 lesions: Does the association of the lesion volume with the prostate-specific antigen density matter in the diagnosis of clinically significant prostate cancer? Urol Oncol. 2021 Jul;39(7):431.e9-431.e13. doi: 10.1016/j.urolonc.2020.11.010

23) Carbunaru S, Stinson J, Babajide R, Hollowell CMP, Yang X, Sekosan M, Ferrer K, Kajdacsy-Balla A, Abelleira J, Ruden M, King-Lee P, Dalton DP, Casalino DD, Kittles RA, Gann PH, Schaeffer EM, Murphy AB. Performance of prostate health index and PSA density in a diverse biopsy-naïve cohort with mpMRI for detecting significant prostate cancer. BJUI Compass. 2021 Jun 15;2(6):370-376. doi: 10.1002/bco2.91

24) Fang AM, Shumaker LA, Martin KD, Jackson JC, Fan RE, Khajir G, Patel HD, Soodana-Prakash N, Vourganti S, Filson CP, Sonn GA, Sprenkle PC, Gupta GN, Punnen S, Rais-Bahrami S. Multi-institutional analysis of clinical and imaging risk factors for detecting clinically significant prostate cancer in men with PI-RADS 3 lesions. Cancer. 2022 Sep 15;128(18):3287-3296. doi: 10.1002/cncr.34355

25) Steinkohl F, Gruber L, Bektic J, Nagele U, Aigner F, Herrmann TRW, Rieger M, Junker D. Retrospective analysis of the development of PIRADS 3 lesions over time: when is a follow-up MRI reasonable? World J Urol. 2018 Mar;36(3):367-373. doi: 10.1007/s00345-017-2135-0

Multitasking Neural Networks for Multiplanar MRI Prostate Localization and Segmentation

Melina Hosseiny, MD[1]; Samira Masoudi, PhD[1]; Christopher Conlin, PhD[1]; Allison Zhong[1]; Tara Retson, MD, PhD[1]; Naeim Bahrami, PhD[1,3]; Sophie You, MD[1]; Troy Hussain[1]; Leonardino Digma[1]; Hafsa S. Babar, MD[1]; Tyler Seibert, MD, PhD[2]; Albert Hsiao, MD, PhD[1]

Abstract

Purpose: Deep learning can be a powerful tool for automating visual tasks in medical imaging, including the localization and segmentation of anatomic structures. However, training these algorithms often requires substantial data curation that may require expert image annotation on multiple imaging planes. For example, the base and apex of the prostate may be more readily marked by radiologists in sagittal planes, while segmentation of central and peripheral zones of the prostate may be more readily handled in axial planes. We thus sought to develop a deep-learning (DL) strategy capable of integrating annotations across multiple imaging planes and hypothesized that it would outperform traditional algorithms developed using single-plane imaging data only.

Materials and Methods: In this retrospective, IRB-approved, HIPAA-compliant study, we collected pelvic magnetic resonance images (MRIs) from 656 male patients. The urinary bladder, prostate, and point locations of the prostate's apex and base were annotated on sagittal T2 images in 391 patients. Central and peripheral zones of the prostate were segmented on axial T2 images in 265 patients. Datasets were then divided by patient into training (80%), validation (10%), and test (10%) cohorts.

Three convolutional neural networks (CNNs) were trained, each based on a U-Net architecture: CNN1 using sagittal images to provide heatmap localizations of the apex and base of the prostate, CNN2 using axial images to segment the prostate and divide it into central and peripheral zones, and a multitask CNN using both data sets to accomplish both tasks. To this end, images and annotations were transformed into a common coordinate system and a custom conditional loss function was incorporated to handle missing labels and encode three-dimensional geometric relationships. Model performance for segmentation and localization was assessed by Dice score and L2 distance error.

Results: Median Dice for whole prostate segmentation improved from 0.803 (IQR 0.76-0.818) by CNN1 to 0.882 (IQR, 0.842-0.890) by the multitask CNN ($p < 0.05$, Wilcoxon test). Mean dice scores for central and peripheral zone segmentation were [81.02 ± 5.58, 63.36 ± 3.96%] respectively by CNN2 and [81.02 ± 5.58 %, 61.67 ± 7.04%] by the multitask CNN respectively without significant difference. Median L2 errors for localization of the base and apex of the prostate decreased from 5.7 (IQR 4.5-6.9) mm and 6.5 (IQR 5.6-7.7) mm by CNN1 to 3.6 (IQR 2.6-4.7) mm and 3.5 (IQR 2.4-4.5) mm by the multitask CNN.

Conclusions: Our proposed multi-task CNN was capable of learning both segmentation and localization tasks, incorporating data from multiple imaging planes, and exceeding the performance of the CNNs trained on individual tasks. These results demonstrate the potential of CNNs for tackling related visual tasks and their potential for combining data from multiple sources or imaging planes.

Keywords: Multitask, Deep learning, Prostate, MRI

Affiliations: [1]Department of Radiology, University of California, San Diego, San Diego, California. [2]Department of Radiation Oncology, University of California, San Diego (UCSD), San Diego, California. [3]GE Healthcare, Menlo Park, California.
Conflict of interest and support statement: The authors declare no competing interests.This study was partially supported through a collaborative research grant with GE Healthcare (AH).
Prior publication: No prior publication of this data has occurred.
Data sharing statement: Deidentified patient data and imaging values are available from the corresponding author upon reasonable request.

Introduction

Medical image segmentation involves partitioning an input image into different segments and aims to delineate the foreground anatomical or pathological structures from the background. Image segmentation helps in the analysis of medical images by highlighting regions of interest, which can be used to define anatomic boundaries, for detection of abnormalities in computer-assisted diagnosis, dose planning for radiotherapy, surgery simulation, and other forms of treatment decision-making. [1]

Manual segmentation by a human expert might seem like the simplest solution to define target boundaries; however, it is a time-consuming and user-dependent process.[2] Because it is such a foundational aspect of so many biomedical problems, segmentation continues to be an important area of ongoing research.[3] Deep learning algorithms, and specifically convolutional neural networks (CNNs), are capable of learning and reproducing an extensive range of parameters, which can then be used to extract features from medical images. [4,5]

In the last several years, deep learning has emerged as a powerful tool for automating segmentation of anatomic structures in medical images. Although each CNN algorithm is generally developed to accomplish a single task, multitask CNNs have the potential to be more computationally efficient. The potential performance benefit of multitask CNNs remains unclear, though few studies have shown improved performance of multi-task algorithms for segmentation and classification of breast tumors on ultrasound and mammography. [6,7]

Image segmentation for prostate MRI can be utilized for a variety of aspects of medical care, including delineation of the gland and zonal boundaries for measurements of prostatic enlargement, procedural planning for prostate biopsies, and radiation therapy planning. [8-10] In addition, algorithms that locate the base and apex of the prostate gland can help to delineate the prostate gland's spatial orientation for automating MRI scan prescription [11,12] and standardizing 3D reconstructions.

However, as with many tasks in medical imaging, certain anatomic structures are better delineated in one plane than another, partly due to anisotropic spatial resolution of multiplanar MRI. For example, the apex and base of the prostate may be more readily delineated in the sagittal plane, and the zonal boundaries of the prostate may be more readily delineated in the axial plane. It remains unclear how to best combine data from multiple imaging planes, and to what degree combining such information is beneficial for CNN performance.

We thus sought to explore the potential of a multitask CNN to combine multiplanar MR images and annotations, and to evaluate its performance for accomplishing two tasks: 1) dividing the prostate into central and peripheral zones, leveraging annotations in axial sections, and 2) localizing the base and apex of the prostate, leveraging annotations in sagittal sections. To that end, we proposed a strategy in which two datasets were aggregated by transforming images and annotations into a common coordinate system and applying a conditional loss function to address missing labels and encode geometric relationships between anatomic structures. We hypothesized that this multitask

Table 1. MR Imaging acquisition parameters for dataset A.

DATASET A, SAGITTAL T2-WEIGHTED IMAGES	
Spatial Resolution (mm x mm)	0.41 x 0.41
Slice Thickness (mm)	3.2
Magnetic Field Strength (T)	3
Repetition Time (ms)	5320
Echo Time (ms)	133
Field of View (cm x cm)	21 x 21
Acquisition Matrix	312 x 253
Flip Angle	137

Table 2. MR Imaging acquisition parameters for dataset B.

DATASET B	SAGITTAL T2-WEIGHTED IMAGES	AXIAL T2-WEIGHTED IMAGES
Spatial Resolution (mm x mm)	0.48 x 0.48	0.46 x 0.46
Slice Thickness (mm)	4	3
Magnetic Field Strength (T)	3	3
Repetition Time (ms)	3747	6197
Echo Time (ms)	102	102
Field of View (cm x cm)	25 x 25	24 x 24
Acquisition Matrix	384 x 352	320 x 320
Flip Angle	111	111

Figure 1. Flowchart of the proposed multi-task CNN and its tasks relative to the single-task CNNs (CNN1 and CNN2). The proposed CNN is trained with a combination of datasets A and B. The component CNNs are trained with the data relevant to their component problems (Dataset A for CNN1, Dataset B for CNN2). Dataset A includes sagittal images of 391 patients with urinary bladder, prostate, and prostate's apex and base annotation while dataset B includes axial images of 265 patients with prostate and its peripheral zone annotation.

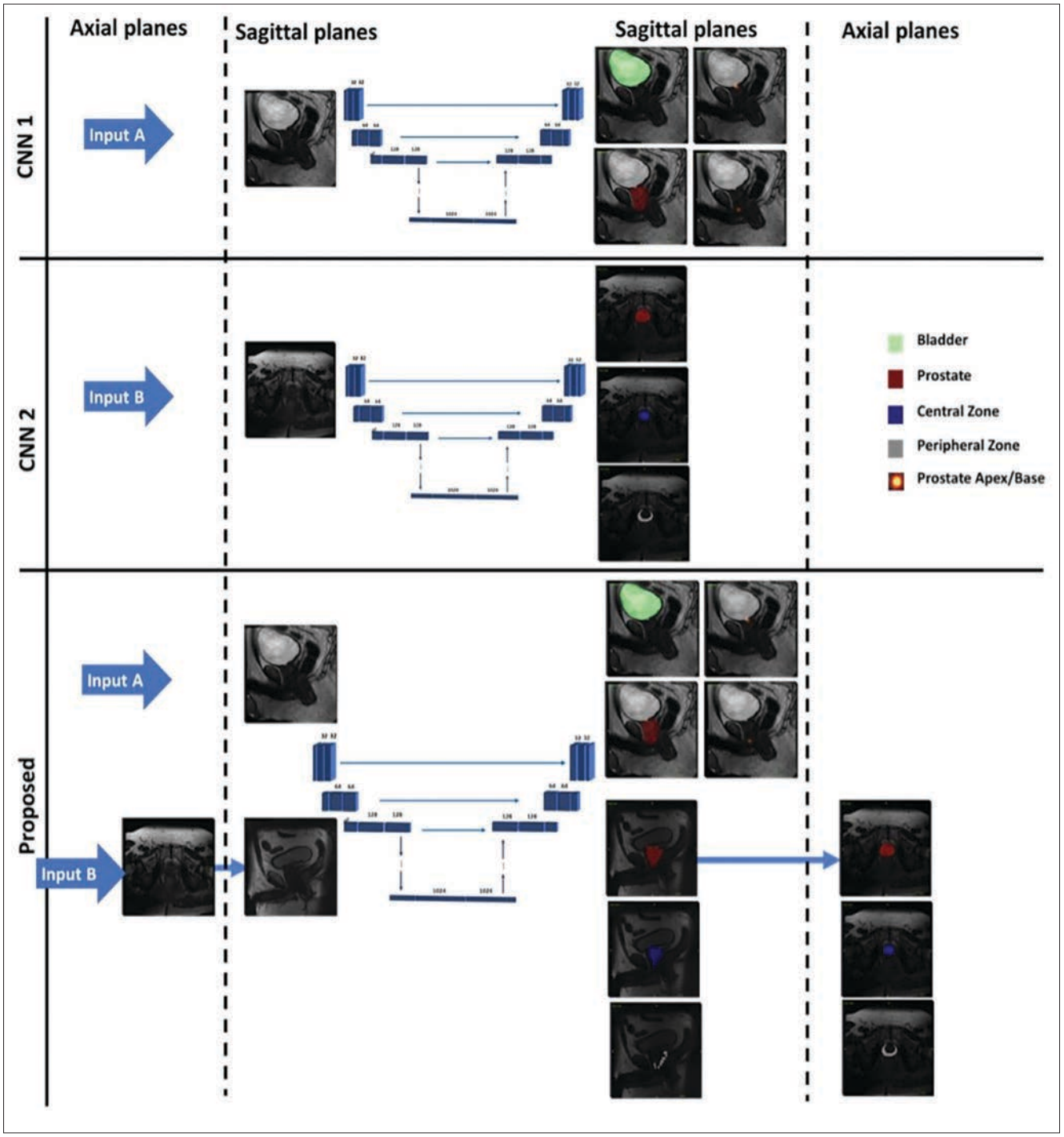

Table 3. Performance of all three CNNs. The proposed multi-task CNN outperforms CNN1 for segmentation and localization on sagittal images and performs comparably to CNN2 for segmentation in axial images.

	Image View	Tasks	CNN 1	Proposed
Dataset A	Sagittal	Bladder segmentation	*88.00 ± 3.10%*	*92.05 ± 2.65%*
		Prostate segmentation	*80.30 ± 6.87%*	*88.19 ± 4.75% **
		Apex localization	*5.66 ± 1.93 mm*	*3.63 ± 1.04 mm ***
		Base localization	*7.26 ± 3.55 mm*	*3.46 ± 1.15 mm **
		Angulation Error (♁)	*14.70 ± 8.60* ♁	*5.91 ± 4.19* ♁
			CNN 2	**Proposed**
Dataset B	Axial	Prostate segmentation	*86.02 ± 2.41%*	*84.00 ± 3.42%*
		Central Zone Segmentation	*81.32 ± 2.55%*	*81.02 ± 5.58 %*
		Peripheral Zone segmentation	*63.36 ± 3.96%*	*61.67 ± 7.04 %*

Wilcoxon signed rank test: * (P-value<0.05), ** (P-value<0.005)

approach would outperform single models separately trained for individual tasks.

Methods

In this retrospective, IRB-approved, HIPAA-compliant study, we collected a convenience sample of pelvic MRIs from 656 male patients (mean age 67 years, range 38-87). Pelvic MRIs were acquired as part of routine clinical care for initial detection, treatment planning, active surveillance of prostate cancer, or to assess for recurrence in previously treated patients with elevated prostate-specific antigen (PSA).

Image Data

Multiparametric MR imaging of the prostate was performed utilizing an MR scanner with a pelvic external phased-array coil using the same standard protocol in accordance with recommendations of ACR and ESUR. The protocol included two-dimensional turbo spin echo (TSE) T2 imaging, three-dimensional dynamic contrast-enhanced (DCE) imaging in three planes, and echo-planar diffusion-weighted imaging (DWI). Tables 1 and 2 show the MRI acquisition parameters.

Image Annotation

Data for this study comprised two datasets. Dataset A included segmentations of the urinary bladder and prostate, and point localizations of the apex and base of the prostate, each annotated on T2 sagittal images from 391 patients. These annotations were performed by a medical student and a radiology resident, supervised by a board-certified radiologist using Arterys (Tempus, USA) software.

Annotations of the apex and base of the prostate were transformed from point localizations to Gaussian heatmaps. Dataset B included segmentations of the prostate gland and its peripheral zone, each annotated on T2 axial images from 265 patients. These annotations were performed by an image analyst and radiology postdoctoral fellow, supervised by a board-certified radiation oncologist. Each dataset was then divided by patient into training (80%), validation (10%), and test (10%) cohorts.

Model Training

Three modified 3D U-Nets were developed with multiple output channels for segmentation and localization tasks. CNN1 was trained using dataset A and a weighted sum of the segmentation and localization loss functions. CNN2 was trained using dataset B and the segmentation loss only. Axial annotations from dataset B were then translated into their sagittal equivalent and combined with dataset A; this combined dataset was used to train the multitask

CNN, incorporating a custom conditional loss function for segmentation and localization in order to 1) ignore missing annotations in the combined dataset, and 2) to take advantage of the morphological relations among the regions of interest. Boundary constraints included the following: (a) central and peripheral zones must sum up to the complete prostate gland; (b) urinary bladder and prostate segmentations must have no overlap, and (c) prostate and base localizations must overlap with the prostate gland segmentation.

In this work, segmentation loss was defined using the Tversky index while localization loss was based on mean square error. For training the single-task CNNs, input images were resampled and zero-padded to (x, y, z) dimensions of 256 x 256 x 16. These images were preprocessed using histogram matching followed by simple image standardization. Augmentation in the form of random image cropping (by -10 to 10 pixels), shifting (by -20 to 20 pixels), and rotation (by -10 to 10 pixels) were applied during neural network training.

Predictions generated by the multitask CNN were compared directly against CNN1 predictions and translated back to the axial plane for comparison against CNN2. Flowchart of the proposed multitask CNN and its tasks relative to the single-task CNNs (CNN1 and CNN2) are shown in Figure 1.

Statistical Analysis

Segmentation performance was assessed using Dice scores (expressed as mean ± SD and/or median along with the interquartile range (IQR)). Localization performance was evaluated using landmark L2 distance error and angulation error, calculated as the error between lines connecting the apex and base of the prostate. Wilcoxon tests were used for comparison of Dice scores, L2 distance error, and angulation error between the evaluated models.

Results

Using two different annotated datasets, three modified 3D U-Nets were trained for segmentation and localization tasks on prostate MRI. Performance of all three CNNs is shown in Table 3.

Prostate Gland Localization

Mean L2 distance error for localization of the prostate gland's apex and base decreased from 5.7±1.92 mm and 6.5 ±2.5 mm by CNN1 to 3.6 ±1.0 mm and 3.5 ±1.2 mm by the multitask CNN. Mean angulation error decreased from 14.7±8.6° by CNN1 to 5.9±4.2° by the multitask CNN (p-value < 0.05). Median L2 distance error for localization of the apex and base of the prostate decreased from 5.7 mm (IQR 4.5-6.9) and 6.5 mm (IQR 5.6-7.7) by CNN1 to 3.6 mm (IQR 2.6-4.7) and 3.5 mm (IQR 2.4-4.5) by the multitask CNN.

Prostate and Urinary Bladder Segmentation

Mean Dice score for prostate segmentation improved from 80.30 ± 6.87% by CNN1 to 88.19 ± 4.75% by the multitask CNN (p-value < 0.05). Median Dice score for prostate segmentation improved from 80.3% (IQR 76.0 - 81.8%) by CNN1 to 88.2% (IQR 84.2 - 89.0%) by the multitask CNN. Mean Dice score for bladder segmentation increased from 88.00 ± 3.10% by CNN1 to 92.05 ± 2.65% by the multitask CNN ($p$value < 0.01). Median Dice score for bladder segmentation improved from 88.99% (IQR 83.78 - 89.97%) by CNN1 to 91.35% (IQR 89.0-93.2%) by the multitask CNN. Our proposed multitask CNN outperformed the single-task CNNs in all segmentation tasks.

Central and Peripheral Zone Segmentation

For central and peripheral zone segmentation, there were no significant differences between the multitask CNN and CNN2 (p-value> 0.05). The mean Dice score for central zone segmentation was 81.02 ± 5.58 % by the multitask CNN and 81.32 ± 2.55% by CNN2. The mean Dice score for peripheral zone segmentation was 61.67 ± 7.04% by the multitask CNN and 63.36 ± 3.96% by CNN2. Two accessions that illustrate multitask CNN performing well are shown in Figure 2.

Discussion

Deep learning is a powerful tool that can be used for the segmentation of anatomic structures in medical imaging, but it typically requires substantial training data that can be time-consuming to obtain. To assess the feasibility of training deep learning algorithms on smaller datasets, we investigated the potential of using multiple datasets, annotated for different purposes on different planes, and aggregated using 3D image re-slicing and image-to-image physical point translation. This is unlike the majority of segmentation approaches presented in the literature which, despite the availability of multi-planar MR images in the standardized protocols, only take axial images into account. The merged dataset was utilized for training a single CNN model, which performed equally well or better than individual models trained using a single dataset.

Figure 2. Representative segmentation and localization of the multitask CNN and comparison against ground truth. Example segmentations by the proposed CNN in representative patients from dataset A and dataset B The case from dataset A shows high agreement with ground truth segmentation: bladder Dice 0.89, prostate Dice 0.86, prostate base localization error of 3.33 mm, and apex localization error of 1.61 mm. The case from dataset B shows high agreement with ground truth with prostate Dice 0.89 and central zone Dice 0.86.

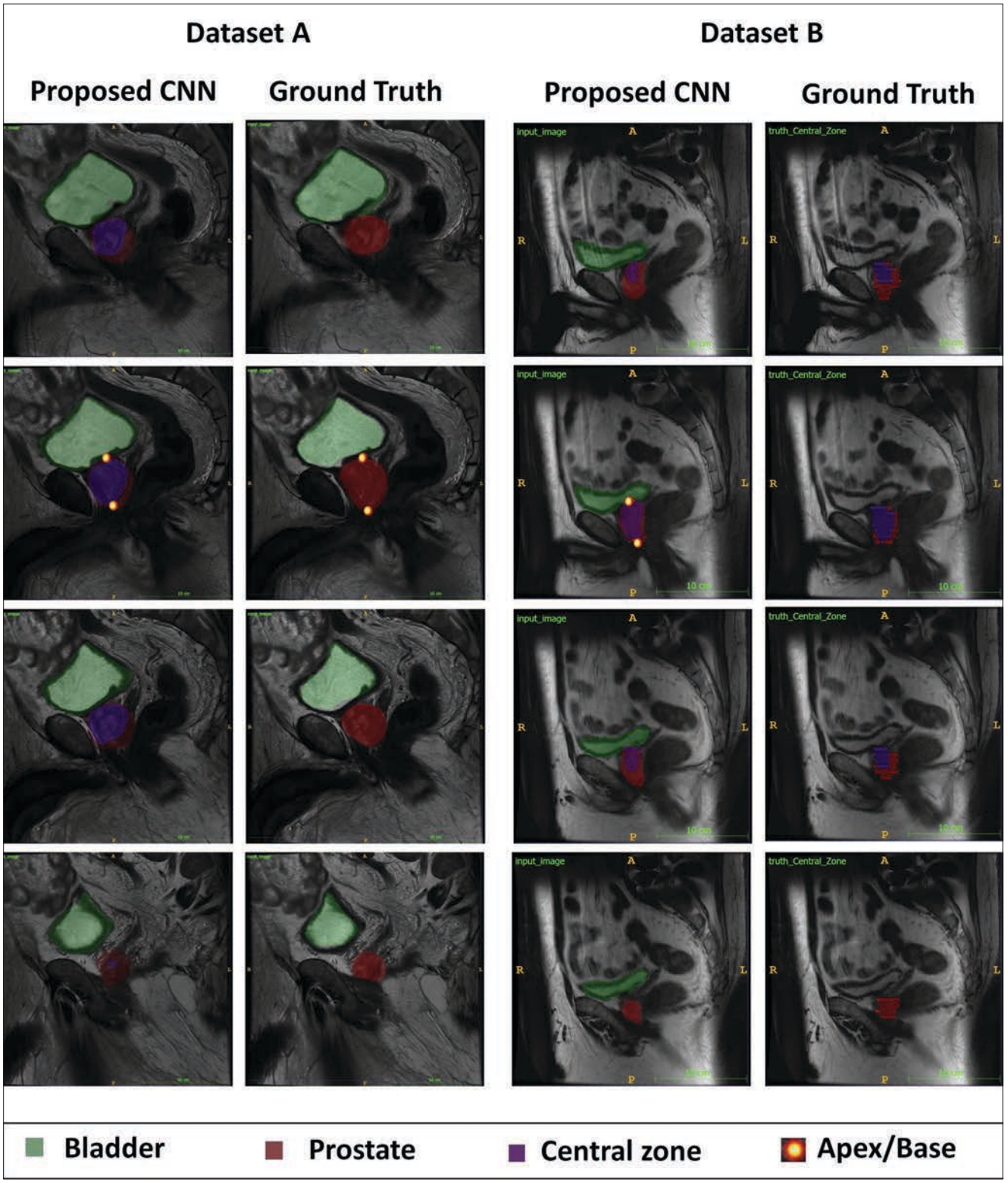

In the present study, our proposed multitask CNN outperformed the single-task CNNs for pinpointing the apex and base of the prostate, which can be used to define the spatial orientation of the prostate gland. This ultimately can be used for separate ongoing work automating oblique plane prescription in MRI.

The multitask model improved prostate gland and urinary bladder segmentation as well as localization of the prostate base and apex. While the annotations required for each task may be more easily acquired in the axial imaging plane, our proposed CNN model was designed to perform all tasks in a single common coordinate system, utilizing conditional loss functions to address missing labels and encode geometric relationships.

The present study is one of the first to investigate whether a fully automated multitask deep learning algorithm can accomplish multiple tasks while merging two annotated datasets, and if so, how this approach might improve the quality of segmentation and localization results. The combined model yielded significantly decreased mean L2 distances and angulation errors for localization of the prostate gland apex and base by 2.1-3 mm and 8.8°, respectively. Improvement in the automated delineation of the prostate gland's craniocaudal orientation can potentially enable a faster automated MR imaging prescription. The multi-task model outperformed each single-task model for segmentation of the prostate gland and urinary bladder boundaries by approximately 8% and 4%, respectively, though it did not show a statistically significant difference in zonal segmentation of the prostate gland.

A number of studies have found satisfactory performance of deep learning algorithms for prostate segmentation at ultrasound and mp-MRI. [13,14] In prior investigations with datasets of 49 to 163 patients, CNN models have obtained Dice similarity coefficients ranging from 0.85 to 0.93 for the automatic segmentation of the prostate gland. [15-18] A study by Tian, et al,[16] applied a deep-learning algorithm for prostate segmentation on a data set of 140 prostate MRIs and yielded a Dice similarity coefficient of 0.85. The online data collection PROMISE12, which contains labeled prostate MR images, has inspired many studies of prostate segmentations. [19] The present study stands up by employing a larger cohort of training datasets, training a multitask deep learning algorithm, and using multiplanar set of images for performing tasks.

Multi-task training relies on sharing features between related tasks to enable the combined model to perform better on the original single tasks. Training deep learning algorithms using small and partially annotated datasets can also potentially overcome the lack of large training datasets by combining images previously annotated for various purposes on different imaging planes, ultimately facilitating the increasing automation of image analysis tasks.

Limitations

We recognize several limitations to this study. Our proposed multi-task CNN model was trained and validated using retrospective data, so our imaging data includes a variety of different vendors, institutions, and imaging techniques. Further work may be essential to ensure comparable results among other scanner manufacturers and institutional protocols. Failure modes of the multitask CNN model may be revealed through more extensive testing, though additional training data would likely enhance performance. The future direction could focus on how well our proposed multitask CNN performs among patients who have aggressive prostate cancer with invasion to seminal vesicles or bladder. Further investigation is needed to determine how well a multitask CNN model will perform in post-operative patients.

Conclusion

In summary, we show that a multitasking CNN approach can successfully be used to aggregate disparate training data developed for multiple tasks in multiple imaging planes. Multi-task deep learning algorithms that utilize such data can outperform component CNNs trained only on data for individual tasks. We believe a similar approach may be used to perform similar tasks for other organs, paving the way to use datasets of more modest size for image analysis of ever-increasing accuracy and complexity.

References

1) Malhotra P, Gupta S, Koundal D, Zaguia A, Enbeyle W. Deep neural networks for medical image segmentation. *J Healthc Eng*. 2022;2022:9580991. doi:10.1155/2022/9580991

2) Comelli A, Dahiya N, Stefano A, et al. Deep learning-based methods for prostate segmentation in magnetic resonance imaging. *Appl Sci (Basel)*. Jan 02 2021;11(2)doi:10.3390/app11020782

3) Liu L, Wolterink JM, Brune C, Veldhuis RNJ. Anatomy-aided deep learning for medical image segmentation: a review. *Phys Med Biol*. 05 26 2021;66(11)doi:10.1088/1361-6560/abfbf4

4) Cai L, Gao J, Zhao D. A review of the application of deep learning in medical image classification and segmentation. *Ann Transl Med*. Jun 2020;8(11):713. doi:10.21037/atm.2020.02.44

5) Bardis M, Houshyar R, Chantaduly C, et al. Segmentation of the prostate transition zone and peripheral zone on mr images with deep learning. *Radiol Imaging Cancer*. 05 2021;3(3):e200024. doi:10.1148/rycan.2021200024

6) Zhou Y, Chen H, Li Y, et al. Multi-task learning for segmentation and classification of tumors in 3D automated breast ultrasound images. *Med Image Anal*. 05 2021;70:101918. doi:10.1016/j.media.2020.101918

7) Chowdary J, Yogarajah P, Chaurasia P, Guruviah V. A multi-task learning framework for automated segmentation and classification of breast tumors from ultrasound images. *Ultrason Imaging*. 01 2022;44(1):3-12. doi:10.1177/01617346221075769

8) Tătaru OS, Vartolomei MD, Rassweiler JJ, et al. Artificial intelligence and machine learning in prostate cancer patient management-current trends and future perspectives. *Diagnostics (Basel)*. 02 20 2021;11(2)doi:10.3390/diagnostics11020354

9) Hosseiny M, Shakeri S, Felker ER, et al. 3-T Multiparametric MRI followed by in-bore mr-guided biopsy for detecting clinically significant prostate cancer after prior negative transrectal ultrasound-guided biopsy. *AJR Am J Roentgenol*. 09 2020;215(3):660-666. doi:10.2214/AJR.19.22455

10) Hosseiny M, Felker ER, Azadikhah A, et al. Efficacy of 3T multiparametric mr imaging followed by 3t in-bore mr-guided biopsy for detection of clinically significant prostate cancer based on piradsv2.1 score. *J Vasc Interv Radiol*. Oct 2020;31(10):1619-1626. doi:10.1016/j.jvir.2020.03.002

11) Guo Z, Li X, Huang H, Guo N, Li Q. Deep learning-based image segmentation on multimodal medical imaging. *IEEE Trans Radiat Plasma Med Sci*. Mar 2019;3(2):162-169. doi:10.1109/trpms.2018.2890359

12) Masutani EM, Bahrami N, Hsiao A. Deep learning single-frame and multiframe super-resolution for cardiac MRI. *Radiology*. 06 2020;295(3):552-561. doi:10.1148/radiol.2020192173

13) Bardis MD, Houshyar R, Chang PD, et al. Applications of artificial intelligence to prostate multiparametric MRI (mpMRI): current and emerging trends. *Cancers (Basel)*. May 11 2020;12(5)doi:10.3390/cancers12051204

14) van Sloun RJG, Wildeboer RR, Mannaerts CK, et al. Deep learning for real-time, automatic, and scanner-adapted prostate (zone) segmentation of transrectal ultrasound, for example, magnetic resonance imaging-transrectal ultrasound fusion prostate biopsy. *Eur Urol Focus*. 01 2021;7(1):78-85. doi:10.1016/j.euf.2019.04.009

15) Clark T, Zhang J, Baig S, Wong A, Haider MA, Khalvati F. Fully automated segmentation of prostate whole gland and transition zone in diffusion-weighted MRI using convolutional neural networks. *J Med Imaging (Bellingham)*. Oct 2017;4(4):041307. doi:10.1117/1.JMI.4.4.041307

16) Tian Z, Liu L, Zhang Z, Fei B. PSNet: prostate segmentation on MRI based on a convolutional neural network. *J Med Imaging (Bellingham)*. Apr 2018;5(2):021208. doi:10.1117/1.JMI.5.2.021208

17) Karimi D, Samei G, Kesch C, Nir G, Salcudean SE. Prostate segmentation in MRI using a convolutional neural network architecture and training strategy based on statistical shape models. *Int J Comput Assist Radiol Surg*. Aug 2018;13(8):1211-1219. doi:10.1007/s11548-018-1785-8

18) Wang B, Lei Y, Tian S, et al. Deeply supervised 3D fully convolutional networks with group dilated convolution for automatic MRI prostate segmentation. *Med Phys*. Apr 2019;46(4):1707-1718. doi:10.1002/mp.13416

19) Litjens G, Toth R, van de Ven W, et al. Evaluation of prostate segmentation algorithms for MRI: the PROMISE12 challenge. *Med Image Anal*. Feb 2014;18(2):359-73. doi:10.1016/j.media.2013.12.002

Low Versus Ultra-High Field MRI: How to Select Your MRI Fleet

Moozhan Nikpanah, MD[1,2]; William R. Willoughby, PhD[3]; Adrienne E. Campbell-Washburn, PhD[4]; Thomas S. Denney Jr., PhD[5]; Ashkan A. Malayeri, MD[2]; Larry ver Hoef, MD[6,7]; Kristin K. Porter, MD, PhD[1]

Abstract

Objective and hypothesis: Magnetic resonance imaging (MRi) is one of the most powerful non-invasive methods for clinical applications as well as biomedical research. Since the mid-1980s, there has been momentum for MRI scanners with higher field strengths to enhance contrast-to-noise ratio, signal-to-noise ratio, and spatial resolution. This resulted in the evolution of 0.3-0.6 Tesla (T) to conventional 1-1.5T and high-field 3T scanners, and eventually, ultra-high field scanners of 7T and beyond. The wide variety of available MR field strengths suits the demand for a multitude of research and clinical applications.

Methods and Materials: A structured literature search was performed for the terms "low-field magnetic resonance imaging" and "ultra-high field magnetic resonance imaging" by mapping their Medical Subject Heading (MeSH) tree structure utilizing the Public Library of Medicine's (PubMed) Automatic Term Mapping (ATM). Then, the PubMed database and the Web of Science (Clarivate Analytics) Core Collection from 1980 to April 2022 were searched using all categories. Some specific searches for relevant topics such as the new MAGNETOM FreeMax MRI system were performed using Google, as well as some further exploration of topics around the future of MRI.

Results: Review articles, original research manuscripts, and editorial materials were reviewed. The selected manuscripts cited in this article represent a comprehensive review of the publications focused on low and ultra-high field MRI and the clinical applications of these systems. Our results showed that each of these MRI systems has unique clinical and research utilities that fit the needs of various healthcare settings or research facilities. Herein, we comprehensively discuss the technical features of these cutting-edge systems, their clinical uses, as well as advantages and disadvantages.

Conclusions: Developing a successful MRI program in a healthcare setting is a complex and comprehensive process that involves financial considerations for equipment procurement and maintenance as well as operational considerations.

Keywords: MRI, Low-Field MRI, Ultra-High Field MRI

Affiliations: [1]Department of Radiology, University of Alabama at Birmingham, Birmingham, AL, USA; [2]Radiology and Imaging Sciences, Clinical Center, National Institutes of Health, Bethesda, MD, USA; [3]University of Alabama at Birmingham, Birmingham, AL, USA; [4]Cardiovascular Branch, Division of Intramural Research, National Heart, Lung, and Blood Institute, National Institutes of Health, Bethesda, MD, USA; [5]Department of Electrical and Computer Engineering, MRI Research Center, Auburn University, Auburn, AL, USA; [6]Department of Neurology, University of Alabama at Birmingham (UAB), Birmingham, AL, USA; [7]Division of Epilepsy, University of Alabama at Birmingham (UAB), Birmingham, AL, USA
Conflict of interest and support statement: Kristin Porter is a stockholder of Pfizer, Inc. Moozhan Nikpanah is a stockholder of NVIDIA and Tesla. This manuscript was not supported by any internal/external sources.
Prior Publication/Presentation: This work was presented at the Partners in Progress Meeting, University of Alabama at Birmingham (UAB), September 25, 2022.
Data availability statement: Data sharing is not applicable as no datasets were generated/analyzed for this study.

Introduction

Magnetic resonance imaging (MRI) is one of the most effective noninvasive diagnostic tools in current medical practice, and it has played a vital role in cutting-edge research, yielding information regarding both structure and function.[1] The early low-field MRI images were at times not interpretable, owing mainly to poor contrast-to-noise ratio (CNR) and signal-to-noise ratio (SNR). Since the mid-1980s, there has been a push for MRI scanners with higher field strength (B0) to solve this limitation by improving CNR, SNR, and spatial resolution.[1,2] These efforts led to the evolution from low-field 0.3-0.6 Tesla (T) scanners with textured images to conventional 1-1.5T and high-field 3T scanners with widespread clinical utilization due to higher image quality and faster acquisition time.[1,3] Application of ultra-high field (UHF, ≥ 7T) MRI in recent years has provided enhanced spatial resolution and improved SNR with decreased voxel size, allowing visualization of smaller structures in detail.[1] However, UHF MRI has its disadvantages, and recently there has been renewed interest in contemporary low-field MRI systems equipped with modern hardware, advanced image acquisition methods, and advanced image reconstruction methods.

Currently, a variety of MRI field strengths are available to meet the need for a multitude of research and clinical utilities. Each of these MRI systems has unique features and capabilities, as well as advantages and disadvantages. In this manuscript, we review the technical aspects of state-of-the-art low, high, and UHF MRI systems and their clinical applications. Additionally, we share recommendations for radiology departments and practices regarding the selection of appropriate technologies that meet the clinical needs of their patient population.

Methods and Materials

A structured literature search was performed for the terms "low-field magnetic resonance imaging" and "ultra-high field magnetic resonance imaging" by mapping their Medical Subject Heading (MeSH) tree structure utilizing the Public Library of Medicine's (PubMed) Automatic Term Mapping (ATM). Then, the PubMed database and the Web of Science (Clarivate Analytics) Core Collection from 1980 to April 2022 were searched using all categories.

Some specific searches for relevant topics such as the new MAGNETOM FreeMax MRI system were performed using Google, as well as some further exploration of topics around the future of MRI. Furthermore, by manual review of the references of these publications, additional references were identified for consideration. After removing the duplicates, the selected manuscripts cited in this article represent a comprehensive review of the publications focused on low-field and ultra-high field MRI, the advantages and disadvantages of these systems, as well as their clinical applications.

Results

Studies in languages other than English were excluded. Review articles, original research manuscripts, and editorial materials were reviewed. The selected manuscripts cited here represent a comprehensive review of the publications focused on low and ultra-high field MRI and the clinical applications of these systems.

Low-Field MRI

The first MRI scanners in the 1980s were low-field, typically with a field strength of 0.25–1.0T.[4] These low-field models had poor spatial resolution, low temporal resolution, and limited image parameters and sequences.[5] When these low-field MRI systems were used in clinical settings, it was assumed, and ultimately verified, that higher static field strengths would improve MRI performance.[4,6]

The MRI signal is proportional to the square of the magnetic field strength, and assuming a constant receive bandwidth, the noise is approximately proportional to the static magnetic field strength (B0). Therefore, the simplest technique to acquire a better SNR in an MRI system is to increase B0; however, B0 does not solely determine the image SNR.[7,8] Developments in MRI technology, including SNR-efficient data acquisitions, parallel imaging, compressed sensing, and machine learning-based image reconstruction methods, have made the imaging methods of low-field MRI systems, which previously were rather restricted, more robust. These sequences are now comparable to those of standard clinical practice on 1.5T MRI systems.[9,10] For example, the National Heart, Lung, and Blood Institute (NHLBI, National Institutes of Health), in collaboration with Siemens Healthineers, ramped down a whole-body 1.5T system to a 0.55T system equipped with high-performance software and hardware.[11] This innovative technology showed significant promise for routine imaging and for novel applications of MRI.

Subsequently, on July 1, 2021, Siemens Healthcare announced that the U.S. Food and Drug Administration (FDA) cleared a 0.55T system (Magnetom FreeMax system

Table 1. Comparison of advantages and disadvantages of low-field and ultra-high field MRI.

LOW-FIELD MRI	
Advantages	**Disadvantages**
▪ Lighter weight ▪ Occupying less space ▪ More portable ▪ Easier Shipping and installation ▪ Patient comfort: -Reduced acoustic noise -Opportunity of open settings in claustrophobic and obese patients ▪ Safety benefits: -Lower torque and translational force associated with ferromagnetic objects -Less heating -Lower risk for implants, endovascular devices, guidewires, and needles ▪ More energy efficient ▪ Reduced susceptibility -Reduced geometric distortion artifacts -Improved imaging near air-tissue interfaces -Improved imaging near-metal ▪ Shorter T1, longer T2, longer T2* -Improved imaging efficiency (ie. shorter TR, longer read-out imaging) ▪ More affordable	▪ Decreased SNR ▪ Decreased CNR ▪ Reduced chemical shift -Challenging fat-suppressed imaging with chemical shift selective (CHESS) pulses -Reduced performance of spectrally selective fat suppression -MRS is more challenging ▪ Less visible contrast enhancement ▪ Reduced susceptibility -SWI is challenging -BOLD effect reduced
ULTRA-HIGH FIELD MRI	
Advantages	**Disadvantages**
▪ Improved SNR ▪ Improved CNR ▪ Increased spectral resolution of MRS -More reliable quantification of metabolites ▪ Longer T1 and shorter T2 at higher fields -Improved chemical exchange saturation transfer imaging ▪ Improved multinuclear MRI ▪ More reliable quantitative MRI for MSK	▪ Patient discomfort -Adverse physiologic effects: metallic taste, nausea, dizziness, vertigo, sweating, and magnetophosphenes -Longer duration, the requirement to lie motionless, and acoustic noise ▪ Artifacts -Inhomogeneities of the B0 field -Inhomogeneities of the radiofrequency (RF) excitation -More probability of motion artifacts -Geometric distortions in EPI BOLD and diffusion-weighted imaging ▪ Shorter T2 relaxation ▪ Increased specific absorption rate (SAR) -More frequent occurrences of RF heating of tissue foci ▪ Signal dropout in SWI at UHF -Negative impact on image quality in certain regions ▪ Frequent need for modification of imaging sequence parameters due to SAR limits ▪ ECG alterations under high magnetic field systems ▪ Lack of commercial coil for all UHF applications ▪ More expensive

by Siemens Medical Solutions Inc., Erlangen, Germany) for clinical applications.[12] This high-performance system combines a 0.55T field strength with sophisticated image processing and deep learning technologies. ViewRay also offers a 0.35T whole-body MRI-linac system with high-performance hardware.[13]

Researchers have developed several dedicated low-field MRI systems and demonstrated significant advantages for portable and point-of-care imaging.[14–16] Hyperfine Research's Swoop System (Guilford, CT) has created a first-of-its-kind portable low-field (0.064T) MRI scanner, which received 510(k) clearance from the FDA in February 2020 and addresses another critical niche for low-field MRI: patient-side imaging.[17] Other application-specific MRI systems include Synaptive's Evry 0.5T head-only MRI system, Promaxo's 0.066T prostate MRI system, and Esaote's MSK MRI systems.[18–20]

Given these considerations, what are currently considered novel low-field MRI scanners have grown in popularity, particularly in areas where higher static field MRI systems are difficult to install or when concerns exist regarding the cost, especially for maintenance.[21]

Advantages and Disadvantages of Low-Field MRI

Diagnostic imaging is a significant cost driver in patient care globally.[5] Therefore, lower costs and simplified installation, operation, and maintenance are required for increased worldwide access.[22] Hospitals also face significant logistical challenges when it comes to site selection.[22] Generally, low-field MRI systems are more lightweight, occupy less space compared to high-field systems, require less shielding, and are more portable.[5,23] This greatly simplifies and lowers the cost and difficulties associated with shipping, installation, and finding an optimal site.[5] There are also patient acceptance benefits: their larger bore diameter allows for a less anxiety-provoking experience for patients with claustrophobia and easier positioning for obese patients.[24]

Imaging in the presence of susceptibility-induced magnetic field inhomogeneities is far superior in low-field; the source of susceptibility can be the lung, bowel, cranial sinuses, or metallic implants. This may afford new clinical opportunities to apply MRI and may improve imaging for the increasing number of patients with implanted devices.[10]

Low-field MRI also provides additional safety benefits. The torque and translational force associated with ferromagnetic objects are lower.[25] Heating is also less of a concern due to the lower specific absorption rate (SAR). The lower magnetic field has the effect of lowering the implant risk profile.[26] These considerations apply to MRI-guided interventions, as well as the associated endovascular devices, guidewires, and needles.[25] This could expand MRI imaging to include cardiovascular interventional procedures, with promising preliminary findings.[27] Some low-field MRI systems still use electromagnets or permanent magnets.[28] For these, simple water cooling might be sufficient, eliminating the need for complicated and costly cryogenic cooling systems used in high-field MRI systems.[23] These advantages highlight how low-field MRI systems may be more energy-efficient and align with environmental sustainability, a topic that has recently been a major focus in the radiology community.[21,29]

On the negative side, low SNR is the most noteworthy limitation of low-field MRI, as previously described. Low SNR can result in reduced image quality, lower resolution, and increased scan time. Although image acquisition, reconstruction, and processing strategies can compensate for the reduced SNR, these are not consistently available. Additionally, in low-field MRI systems (up to 0.3T), the application of fat-suppressed imaging with chemical shift selective (CHESS) radio frequency (RF) pulses is challenging.[30,31] This is due to the decreased chemical shift of water and fat spectra at lower field strengths, which makes the application of fat suppression pulses more difficult. Exacerbating this, the water spectral width expands in an inversely proportional ratio to T2*, and the water signal can be inadvertently readily suppressed even with minor inhomogeneities in the magnetic field.[31]

Magnetic susceptibility is proportional to field strength, and while this is advantageous for reduced artifacts in many sequences, it is a challenge for others.[23] As a result, 3T is widely accepted as the preferred field strength for some clinically significant MRI studies, including time of flight (TOF) MRI angiography (MRA) and susceptibility-weighted imaging.[26] However, more recently, TOF MRA and susceptibility-weighted imaging have been acquired with image quality comparable to the 3T studies using the high-performance 0.55T low-field systems.[23] Also, while still evolving, the current opinion is that the acquisition time on the 0.55T low-field systems can also be kept constant compared to 1.5T systems by leveraging SNR-efficient acquisitions and utilizing advanced reconstruction techniques.

Diffusion-weighted imaging (DWI) provides qualitative and quantitative information regarding tissue cellularity. The b-value is directly related to water diffusion

Figure 1. Axial multisection imaging using T2 fBLADE MRI (1.1 × 1.1 × 6 mm^3) in a patient following recovery from COVID-19 infection.

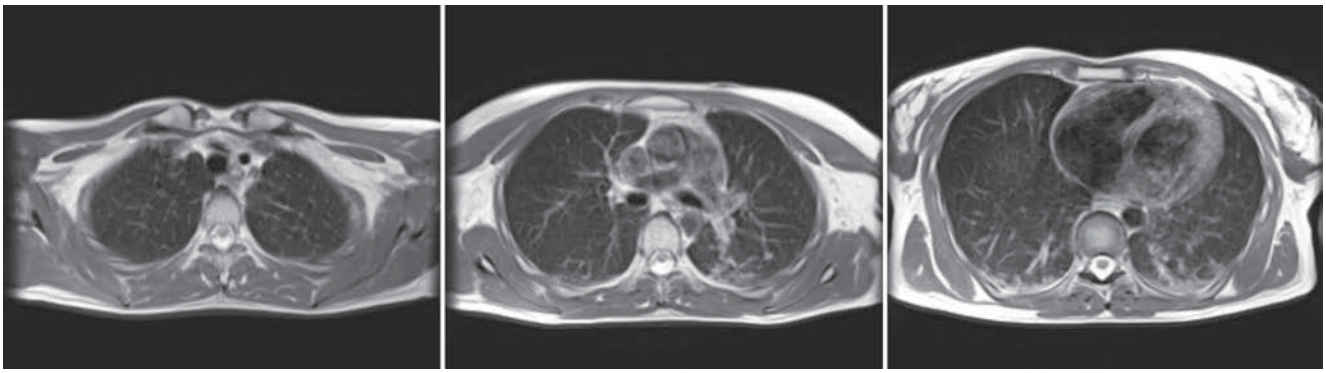

effects and reflects the strength and timing of the gradients used to generate diffusion-weighted images. High-performance gradient systems with high maximum gradient amplitudes and slow rates result in increased spatial resolution and faster acquisitions; however, at higher field strengths, susceptibility and T2* effects are greater. At lower field strengths, imaging parameters for DWI may be manipulated such that it is possible to acquire similar high-quality images (eg, time to echo and readout bandwidth).

Clinical Applications of Low-field MRI

Low-field MRI has applications across body systems such as musculoskeletal (MSK), lung, cardiovascular, and abdomen. As initially investigated at the NIH, comprehensive lung imaging using high-performance low-field MRI provides novel imaging data to complement existing standard assessments such as spirometry, exercise testing, and CT. For instance, MRI measures of regional ventilation-perfusion (VQ) mismatch would be preferable over nuclear imaging approaches, which have limited resolution and are frequently unavailable.[32] Oxygen-enhanced MRI has shown particular promise in low-field, where the T1 relaxivity of oxygen is higher.[33,34]

Compared to the current clinical workflow, in which patients are imaged multiple times with CT imaging, MRI tissue characterization provides higher specificity and lower radiation exposure on serial lung imaging.[32] Recent studies have demonstrated high-quality structural lung imaging and similar pulmonary findings on high-performance MRI images and CT studies in several patients, including patients with COVID-19, suggesting the potential for repetitive lung assessments in these patients.[35–38] Since MRI does not emit ionizing radiation, the ability to acquire MRI images with high quality is important in the pediatric population and may have clinical applications for younger patients with chronic pulmonary diseases, such as cystic fibrosis.[32] Low-field MRI offers a specific advantage for lung imaging due to the reduced susceptibility of the air in the lung parenchyma (Figure 1).

New low-field MRI has been applied to cardiovascular imaging and provides accurate and consistent clinical measurements for cine and late gadolinium enhancement imaging (Figure 2).[39,40] Additionally, low-field MRI offers advantages for MRI-guided cardiovascular catheterization and interventional research.[40,41] Heating of implanted materials may also be reduced in low-field MRI as compared to high-field given the lower SAR; although, questions regarding the impact of implant length, shape, orientation, insulation, and position with respect to the transmit coil at low-field remain incompletely explored to date. [21]

Low-field imaging may be a preferable MRI technique for joint imaging,[42] particularly when considering the reduced artifacts around implants. A study by Reil, et al, showed that the 0.2T MRI method has low sensitivity but high specificity for articular cartilage lesions.[43] Field strengths <100mT have demonstrated even more improvement in metallic artifacts.[44] Low-field MRI has also been applied for diagnostic abdominal MRI and for quantification of iron overload (Figure 3).[45,46]

One important factor in utilizing imaging modalities in clinical settings is their accessibility. Hyperfine Research's Swoop portable system makes MRI available and accessible.[17] This novel system has beneficial utility in time-sensitive and point-of-care settings such as intensive care units, emergency rooms, and mobile stroke units.[47] Portable MRI has the potential for neuroimaging of brain injuries, intracranial hemorrhage, hydrocephalus, and midline shift in high-risk clinical settings.[48,49] Portable MRI systems may significantly expand the role of MRI in a variety of settings.

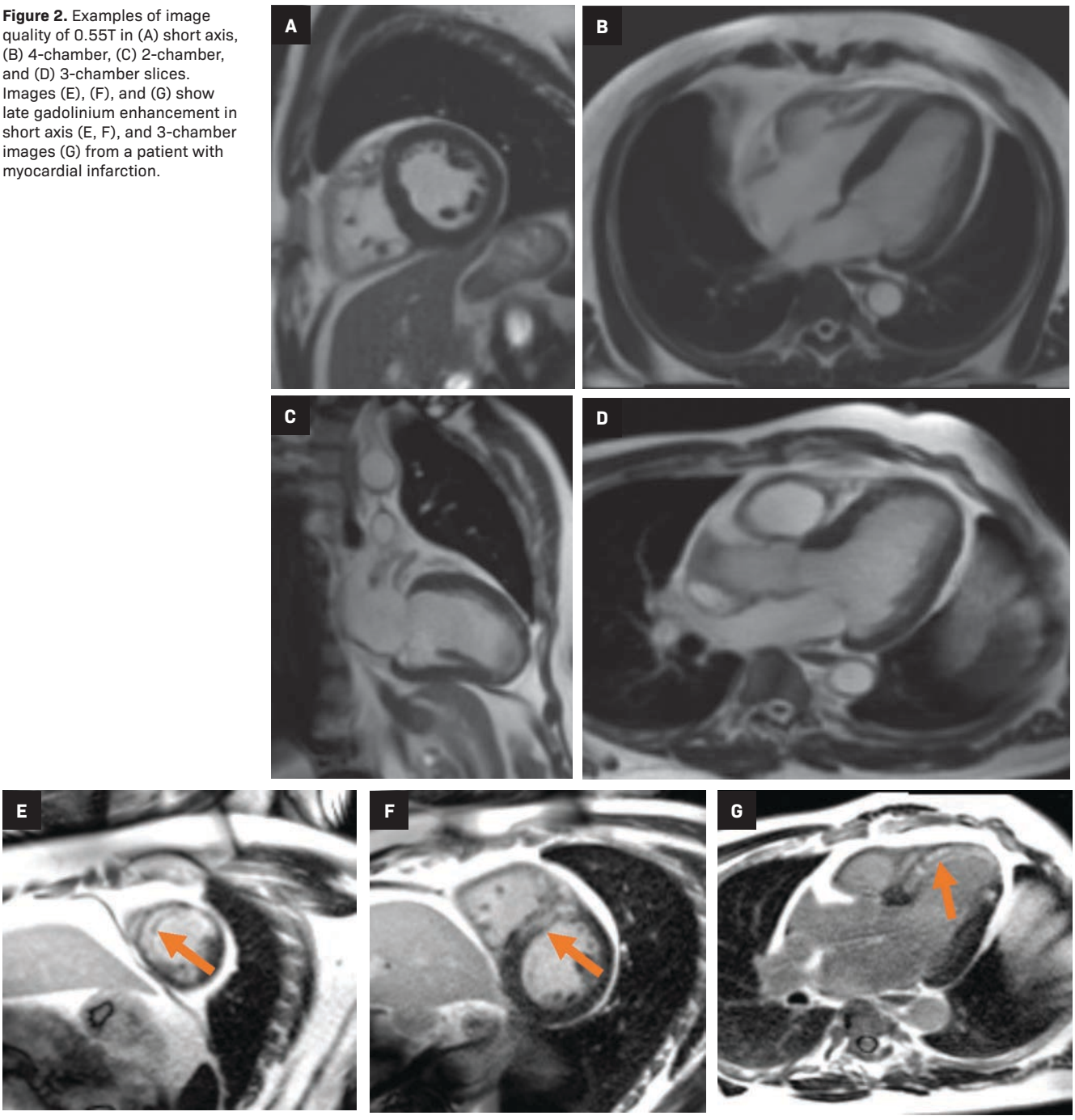

Figure 2. Examples of image quality of 0.55T in (A) short axis, (B) 4-chamber, (C) 2-chamber, and (D) 3-chamber slices. Images (E), (F), and (G) show late gadolinium enhancement in short axis (E, F), and 3-chamber images (G) from a patient with myocardial infarction.

Ultra-high Field MRI

While the majority of MRI examinations are currently performed at static magnetic fields of 1.5 and 3T, systems with higher fields up to 10.5T have been used for research purposes, particularly in neuroscience, since the late 1990s.[50–52] In 1998, the first human MRI study using UHF (MRI scanners with field strength of ≥ 7T) was performed at Ohio State University on an 8T scanner.[53] The results were remarkable, leading to the installation of several UHF research scanners across the world. Moreover, after the FDA declaration in 2014 classified MRI up to 8T as a negligible risk, in 2017, the first 7T system with FDA 510(k) clearance hit the market (Magnetom Terra system by Siemens Medical Solutions Inc., Erlangen, Germany) for clinical use, confined

Figure 3. Examples of image quality of 0.55T in abdominal imaging (A) T2 Trufi, (B) T1 VIBE Dixon In Phase, (C) T1 VIBE Dixon Out Phase, (D) DWI b=400, and (E) T2fBLADE in a healthy volunteer

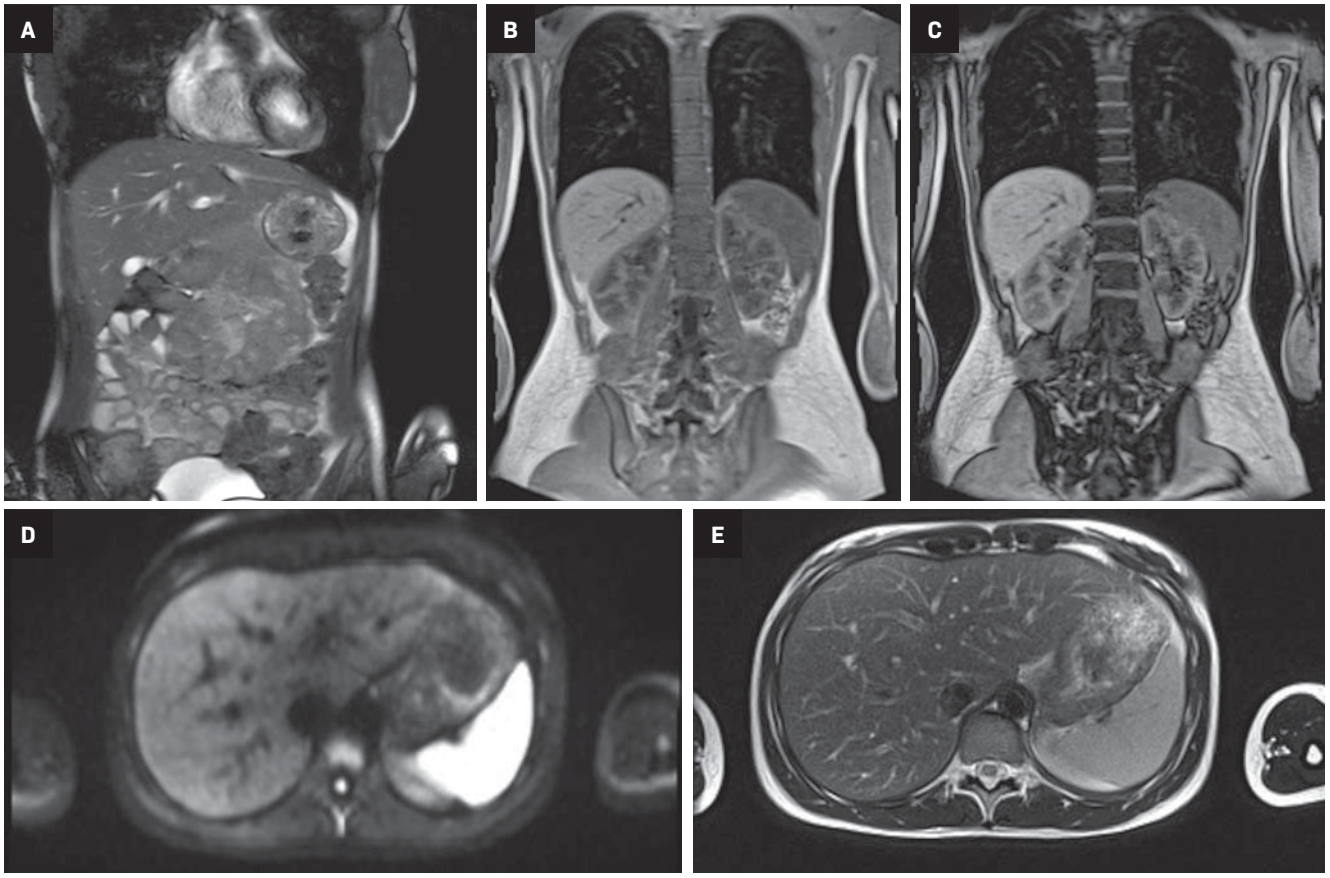

to examination of the head, and upper and lower extremities (neuro and MSK).[54,55]

As of 2018, sixty-two 7T human scanners were installed worldwide, and eight more 7T scanners were on order. Five 9.4T human scanners had been installed in Minnesota, Chicago, Tübingen, Jülich, and Maastricht. Moreover, several human scanners >10T had been installed or were in development, which included whole-body 10.5T (Minnesota), head-only 11.7T (Bethesda), whole-body 11.7 T (Paris), and 14T (Heidelberg).[56–58]

Advantages and Disadvantages of UHF MRI scanners

Improved SNR is the most commonly cited reason for justifying the expenditure and effort of obtaining higher magnetic field scanners. Many MRI applications can benefit from the increase in SNR associated with higher magnetic fields through better spatial resolution or, in the case of dynamic processes, higher temporal resolution.[2] Higher SNR at UHF MRI also allows for higher resolution and/or high b-value acquisition on DWI.[59] SNR is not always the most important measure to assess the potential of MRI to identify lesions of interest; CNR is a more precise parameter for this purpose.[2]

A wide range of imaging features are affected by field strength, and many MRI applications benefit from the resultant increase in both SNR and CNR. Enhanced contrast in susceptibility-weighted imaging (SWI) at higher fields is due to increased phase shifts at higher Larmor frequencies, and stronger blood oxygen level-dependent (BOLD) contrast on functional MRI (fMRI) is due to greater susceptibility (T2*) effects at higher field strengths.[60] Improved CNR also leads to improved magnetic resonance spectroscopy (MRS) SNR and enhanced separation of MRS peaks/spectral resolution.[61] Moreover, T1 is longer and T2 is shorter at higher fields, resulting in improved chemical exchange saturation transfer (CEST) imaging.[62, 63]

Structural MRI is based on the ^{1}H MR signal from water molecules (H_2O). Proton MRS (^{1}H MRS) plays a complementary role to conventional MRI by delivering a plethora of biochemical and metabolic data.[64] Multi-nuclear MRI captures MR sig-

nal from nuclei other than hydrogen such as sodium-23 (^{23}Na), phosphorus-31 (^{31}P), fluorine-19 (^{19}F), and carbon-13 (^{13}C). Because these nuclei are involved in many biological processes, they provide metabolic and functional information beyond that provided by hydrogen alone. Because these nuclei occur at a relatively low concentration, the increased signal available from UHF MRI systems has improved the ability to image using these physiologically relevant nuclei.[65]

Some of the challenges of UFH include inhomogeneities of the B0 field, inhomogeneities of the radiofrequency (RF) excitation, shorter T2 relaxation, and increased SAR.[66] Technical developments such as improved coil designs, higher-order B0 shimming, radiofrequency pulse shaping (B1 shimming), and parallel transmission techniques can address some of these challenges (2), but others like shorter T2 and increased SAR are physical limitations that cannot be solved through engineering.

Moreover, even though UHF provides images with higher resolution and enhanced differentiation of tissue types, motion artifacts are more likely to appear on high-resolution MRI.[67] A variety of prospective and retroactive motion correction approaches have been applied to address this concern.[68,69] The increased occurrence of signal dropout in SWI at UHF, which is advantageous for certain clinical applications like the detection of microbleeds and other small lesions, negatively impacts image quality in certain regions of interest near air-tissue interfaces.[2] Geometric distortions in EPI BOLD and diffusion-weighted imaging are also increased at UHF, which can offset gains in spatial or temporal resolution without special post-processing steps.[70,71]

Physiologically, at UHF there are more frequent occurrences of RF heating of tissue foci. Therefore, to stay compliant with regulatory standards, imaging sequence parameters must frequently be modified, such as repetition time lengthening or lowering the number of captured slices, which makes clinical utilization of UHF extremely challenging.[2] The physiologic effects of higher magnetic fields are time-dependent and can be classified as transient or permanent. Transient effects vanish either promptly or in a reasonably short amount of time post-exposure and affect the daily function of body systems, whereas permanent consequences cause prolonged health concerns.

Some of the transient physiologic effects of UHF MRI systems include metallic taste, nausea, dizziness, vertigo, sweating, and magnetophosphenes.[2,72] With the development of UHF systems, concerns exist that uncomfortable transient symptoms might impact patients' desire to undergo imaging studies. Therefore, several studies comprehensively investigated these outcomes on 7T and 9T systems and reported that even though these effects were higher in high magnetic fields compared to lower fields, they had no major impact on the technique's acceptability.[72,73] However, the most observed causes of discomfort in patients were study duration, the requirement to lie motionless, and acoustic noise, which were irrelevant to magnetic field strength.[73]

Another important effect is electrocardiogram (ECG) alterations under high magnetic field systems, marked by high T-waves.[74] Such ECG variations can make it challenging to interpret UHF imaging sequences that rely on cardiac triggering or gating. There has also been debate in the literature regarding whether UHF systems may impact blood pressure as a result of the extra effort to circulate blood through the high magnetic field. Initial modeling studies suggested this would pose a possible obstacle to 10T or higher MRI examinations; however, subsequent studies on humans and animals assessing blood pressure variations when exposed to high magnetic fields indicated no meaningful consequences at fields as high as 9.4T or 10.5T.[75–77]

Multiple investigational studies have also focused on temporary cognitive consequences, with some studies concluding no correlation while others reporting a positive correlation.[78–81] Even though occupational exposure to magnetic fields is often far lower than the high field at the isocenter of the magnet, employees who are involved in maintaining or cleaning the interior of the machine may be subjected to high fields. Studies are ongoing regarding these effects and approaches to minimize potential negative outcomes.

Long-term or permanent effects of high magnetic fields are mainly assessed by evaluating DNA damage. According to the International Commission on Non-Ionizing Radiation Protection (ICNIRP) and most recent scientific reports and reviews, the possible effects of MRI on DNA are far lower than ionizing radiation outcomes.[82,83] Few investigations have studied the effect of MRI on DNA, with controversial findings.[84,85] In-vivo and in-vitro investigations on strength fields as high as 7T and large study populations found no substantial DNA alterations.[84,86,87] MRI has been widely used to evaluate many patients, with an outstanding record for safety, even at 7T. Studies with larger patient populations are warranted to evaluate the safe utilization of even higher magnetic field strengths.

Figure 4. Side-by-side comparison of (A) 3T (2.0x2.0x2.0 mm^3,TR: 3000ms) and (B) 7T (0.85x0.85x1.5 mm^3, TR: 3000ms) EPI BOLD in a healthy volunteer.

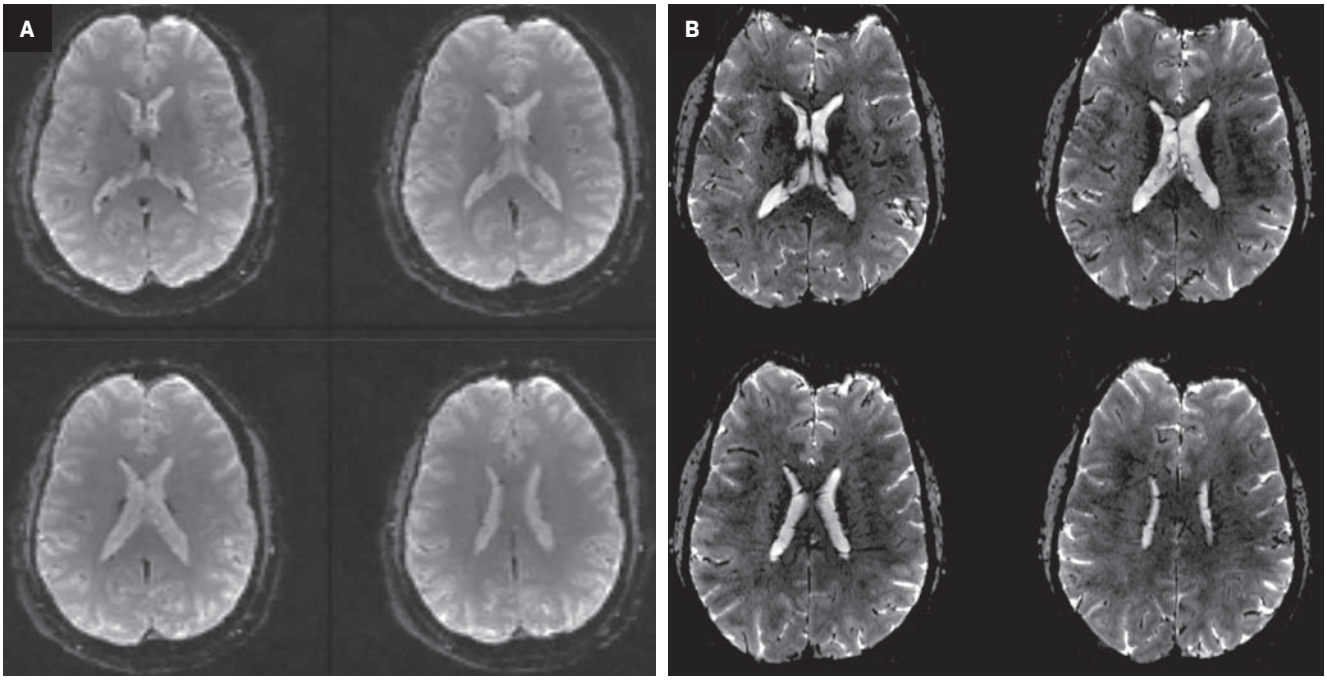

Figure 5. Side-by-side comparison of (A) 3T (1.0x1.0x1.0 mm^3,TA: 4:17) and (B) 7T (0.7x0.7x0.7 mm^3,TA: 6:35) MPRAGE in a healthy volunteer.

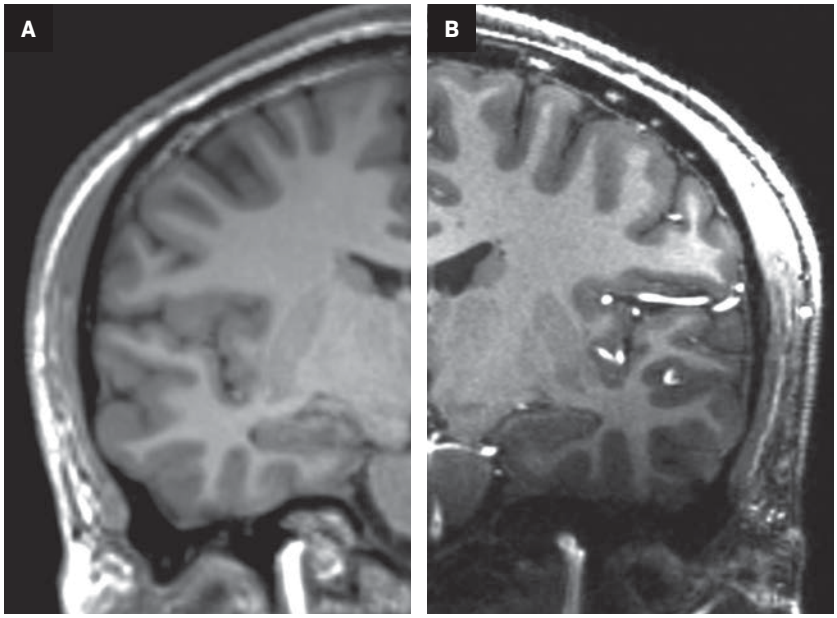

In addition, UHF scanners have much higher initial and operational expenses than non-UHF scanners. Low manufacturing volumes, as well as the expenditures involved in creating a strong magnetic field, such as magnets and conductors, greatly increase the cost of these scanners. The higher magnetic field contributes significantly to the scanners' operational costs by increasing shielding and site preparation expenditures.[88] Moreover, due to the current lack of efficient body coils for UHF scanners, transmit/receive coils must be utilized, which further increases the overall cost.[89]

Clinical Applications of UHF MRI

There is growing data on the potential of UHF MRI in improving diagnoses and clinical management of several pathologies. In neuroradiology, UHF MRI's higher resolution has been shown to enhance the representation of detailed and complex anatomical structures,

Figure 6. Side-by-side comparison of (A) 3T (1.0x1.0x1.0 mm^3,TA: 4:17) and (B) 7T (0.7x0.7x0.7 mm^3,TA: 6:35) MPRAGE in a healthy volunteer.

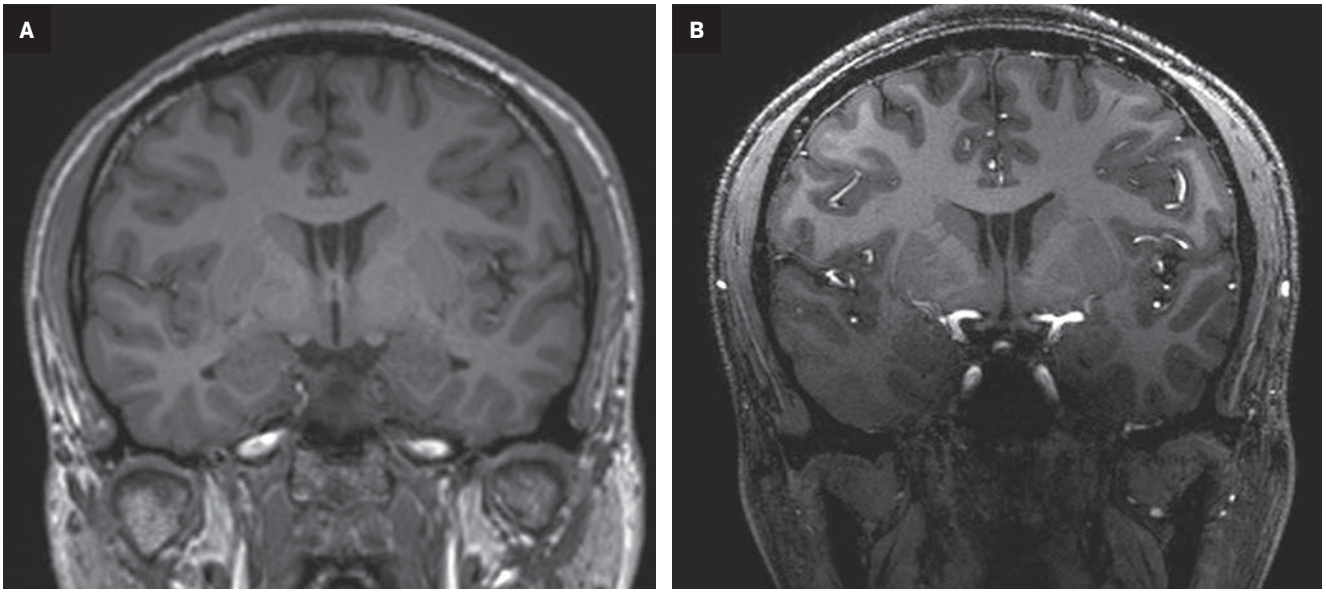

such as cranial nerves and structures of the brain stem (Figures 4, 5, 6).[90,91] UHF MRI enables better detection of arteriovenous malformations (AVMs) and cerebral microaneurysms with diameters of 1 mm or smaller.[92,93] In individuals with stroke, small infarctions not identified on 1.5T MRI were detected on 8T MRI images utilizing weighted gradient echo (GRE) and rapid acquisition with relaxation enhancement.[94] For patients with multiple sclerosis, recent studies have shown increased diagnostic confidence using UHF MRI compared to 1.5T or 3T (Figures 7 and 8).[95] 7T MRI has also shown utility in neurodegenerative diseases such as Alzheimer's disease by providing an accurate volumetric evaluation of hippocampal subfields and the entorhinal cortex.[96] Moreover, UHF MRI at 7T could be used to better visualize the substantia nigra and its inner structure in patients with Parkinson's disease.[97] In epileptic patients, UHF MRI systems enable better visualization of epileptic foci by improving SNR and CNR.[98,99] The higher spatial resolution of 7T scanners provides the opportunity to better detect and distinguish brain tumors from surrounding tissues.[100]

In addition to neuroradiology applications, 7T scanners have been approved for a number of musculoskeletal indications. Trabecular bone microarchitecture has been evaluated by using GRE-based pulse sequences and high-resolution spin-echo applied to 7T, leading to enhanced visualization of tissues.[101] When the diagnostic performance of 7T was compared to that of 3T in the diagnosis of joint diseases in individuals with knee pain, 7T not only showed considerable improvements in SNR but also enhanced overall diagnostic confidence, particularly for the evaluation of small joint structures.[102] T2 and T2* mapping at 7T have demonstrated a positive correlation with water content on the evaluation of cartilage collagen matrix integrity.[103] Moreover, T1ρ imaging at 7T MR, which is utilized in the evaluation of proteoglycan content in cartilage, has led to improved sensitivity with the same resolution compared to 3T MRI scanners.[104] The feasibility of spine MRI at UHF has been described in prior studies, and recent advances in innovative coil technology enhance 7T spine MR by increasing SNR.[105,106]

In comparison to neuroimaging and MSK applications, a limited number of studies have focused on the application of UHF MRI in abdominal and thoracic imaging. Ladder et al. reported that the improved SNR and CNR at 7T seen in a variety of abdominal organs allowed the identification of minor pathologies that would otherwise be undetected at lower field strengths.[107] The feasibility of good-quality images of the kidneys has been shown at 7T, especially T1 GRE MRI.[108] Umutlu, et al, demonstrated that contrast-enhanced MRI cholangiopancreatography (MRCP) is feasible at UHF. The authors reported equivalent results compared to 3T MRCP.[109] In prostate MRI, T2 and DWI (± dynamic contrast-enhanced) are the most frequently used sequences. By applying high-resolution T2 TSE MR at 7T, cancerous lesions in both the transition zone and the peripheral zone could be distinguished.[110] 7T has also shown feasibility in the assessment of breast cancer lesions and in cardiac MRI.[111–113]

Figure 7. A patient with relapsing-remitting multiple sclerosis. (A) Fluid-attenuated turbo inversion recovery magnitude (TIRM), (B) T2, (C) T2*.

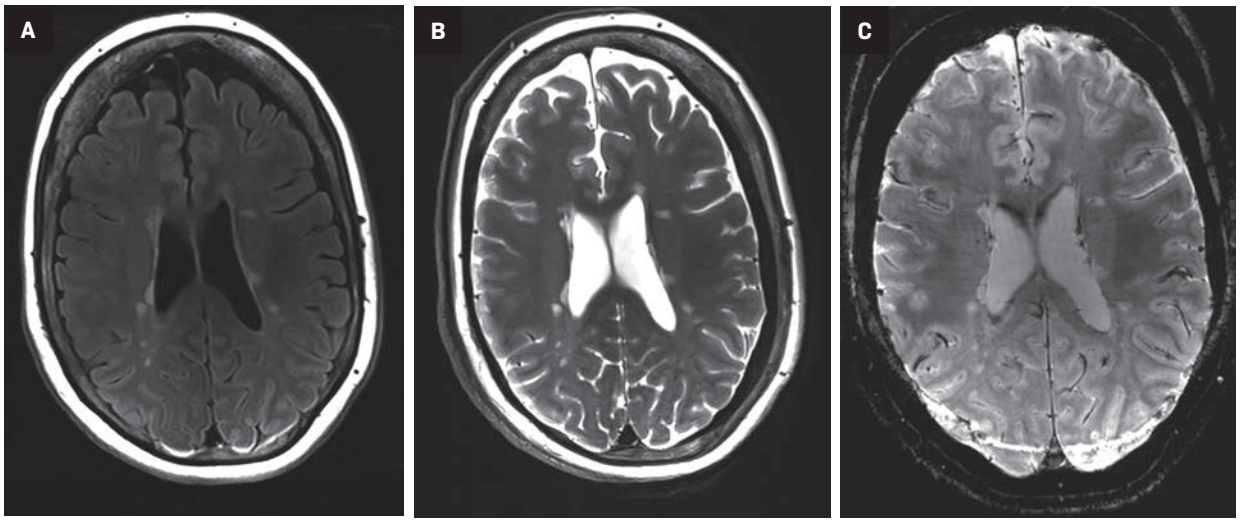

Figure 8. A patient with relapsing-remitting multiple sclerosis. (A) Axial and (B) sagittal fluid-attenuated turbo inversion recovery magnitude (TIRM), 0.7x0.7 mm^2, 1.9 mm slice thickness.

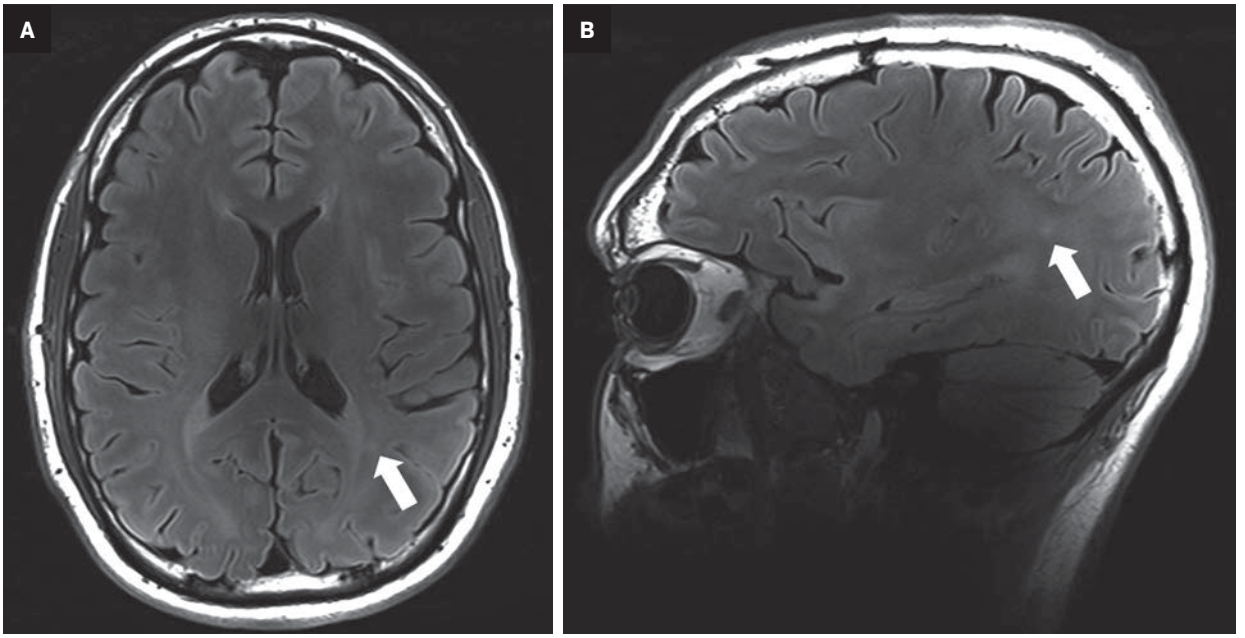

Discussion

Developing a successful MRI service in a healthcare setting is a complicated and multifaceted process that includes financial considerations for equipment purchases, maintenance, and upgrade contracts, as well as operational considerations for safety, quality assurance, and workflow. Additionally, an MRI technologist with expertise in image acquisition and operating logistics specific to the scanner is also required. Therefore, it is crucial to comprehend the opportunities and challenges of each scanner, and the selection of an MRI scanner should consider all of these factors.

Academic Institutions and Research Facilities

Increased SNR and CNR, high spatial resolution, and improved image quality of UHF systems provide the opportunity for better visualization of detailed and complex pathologies. This feature makes UHF MRI ideal for understanding the pathophysiology and investigating the natural history of various disease processes.

On the other hand, low-field MRI systems have great potential for research, particularly related to new applications of these systems and clinical validation of emerging

sequences and techniques. Capabilities unique to low-field settings, such as their mobility, increase access and make imaging investigations possible in previously uninvestigated situations, such as the ICU.

Community-based Inpatient Facilities and Hospitals

Mainstream imaging studies are performed on 1.5-3T scanners, as these are the most standardized in terms of acquisition protocols and radiology technologists' familiarity. Moreover, radiologists are more accustomed to interpreting the images acquired by these scanners.

Low-field scanners can help with intraoperative imaging in community-based inpatient hospitals. The intraoperative application of these scanners in such settings facilitates multidisciplinary communication and provides the opportunity for better patient care in situations requiring urgent and emergent clinical decision-making. Additionally, the portability feature can alleviate many logistical challenges for patient transport in and out of specific hospital wards. The low cost of low-field scanners might be especially beneficial for inpatient facilities looking to grow their MRI fleet. Many of the routine exams conducted in radiology today do not benefit from the features afforded by higher fields such as 3T. These exams might be offloaded to a less expensive low-field system, freeing up higher field strength scanners for applications that benefit from them.

The presence of UHF scanners in the MRI service of a community-based inpatient facility could potentially improve patient care in clinical scenarios that require higher resolution imaging for enhanced interpretation, accurate diagnosis, and therefore optimal management. However, the relatively limited benefits in this setting need to be balanced with the operational challenges and the cost associated with the maintenance of these scanners.

Private Practice Radiology Settings

Low-field MRI systems are well suited for private practice settings due to their low cost and ease of maintenance. As the cost of an MRI scanner is directly associated with the magnet strength, low-field scanners have lower initial purchase costs. Moreover, owing to decreased energy consumption and safety considerations, these systems require less maintenance cost.

Low-field MRI systems may also broaden the potential patient population for radiology private practice settings; for example, claustrophobic patients and individuals who have difficulty staying in closed MRI systems due to their body habitus may prefer radiology practices that offer more open configuration MRI imaging options. Additionally, the reduced noise associated with low-field systems may result in less anxiety and an improved imaging experience, enhancing value-based care.

Conclusion

Selecting an MRI scanner for a private practice setting, tertiary care institution, or research center is a nuanced task. In order to make an informed decision, it is critical to evaluate the imaging scenarios for which the scanner is intended and in which it excels, as well as a comprehensive understanding of the strengths and limitations of various magnetic fields.

References

1) Barisano G, Sepehrband F, Ma S, et al. Clinical 7 T MRI: Are we there yet? A review about magnetic resonance imaging at ultra-high field. *Br J Radiol*. 2019;92(1094):20180492.

2) Ladd ME, Bachert P, Meyerspeer M, et al. Pros and cons of ultra-high-field MRI/MRS for human application. *Prog Nucl Magn Reson Spectrosc*. 2018;109:1-50.

3) Alvarez-Linera J. 3T MRI: advances in brain imaging. *Eur J Radiol*. 2008;67(3):415-426.

4) Marques JP, Simonis FFJ, Webb AG. Low-field MRI: An MR physics perspective. *J Magn Reson Imaging*. 2019;49(6):1528-1542.

5) Sarracanie M, Salameh N. Low-Field MRI: How Low Can We Go? A Fresh View on an Old Debate. *Frontiers in Physics*. 2020;8. doi:10.3389/fphy.2020.00172

6) Przyborowska P, Adamiak Z, Holak P, Zhalniarovich Y. Comparison of Feline Brain Anatomy in 0.25 and 3 Tesla Magnetic Resonance Images. *Anat Histol Embryol*. 2017;46(2):178-186.

7) Fischer A. Revisiting the Physics behind MRI and bhe Opportunities bhab Lower Field. https://cdn0.scrvt.com/39b415fb07de4d9656c7b516d8e2d907/395bbaf693bcd08d/57c490bfbb34/sh-1624_MAGNETOM_Flash_Free-Max_Edition_K4_fischer.pdf

8) Choquet P, Breton E, Goetz C, Marin C, Constantinesco A. Dedicated low-field MRI in mice. *Physics in Medicine and Biology*. 2009;54(17):5287-5299. doi:10.1088/0031-9155/54/17/014

9) Klein HM. *Clinical Low Field Strength Magnetic Resonance Imaging: A Practical Guide to Accessible MRI*. Springer; 2015.

10) Campbell-Washburn AE, Ramasawmy R, Restivo MC, et al. Opportunities in Interventional and Diagnostic Imaging by Using High-Performance Low-Field-Strength MRI. *Radiology*. 2019;293(2):384-393.

11) Campbell-Washburn AE, Jiang Y, Körzdörfer G, Nittka M, Griswold MA. Feasibility of MR fingerprinting using a high-performance 0.55 T MRI system. *Magnetic Resonance Imaging*. 2021;81:88-93. doi:10.1016/j.mri.2021.06.002

12) Hamilton-Basich M. FDA Clears Siemens Healthineers Magnetom Free.Max 80 cm MR Scanner. *AXIS Imaging News*. Published online July 7, 2021. https://search.proquest.com/openview/8159ee793b68825befd794cfc51b2de1/1?pq-origsite=gscholar&cbl=2037571

13) Klüter S. Technical design and concept of a 0.35 T MR-Linac. *Clin Transl Radiat Oncol*. 2019;18:98-101.

14) Cooley CZ, McDaniel PC, Stockmann JP, et al. A portable scanner for magnetic resonance imaging of the brain. *Nat Biomed Eng*. 2021;5(3):229-239.

15) O'Reilly T, Teeuwisse WM, de Gans D, Koolstra K, Webb AG. In vivo 3D brain and extremity MRI at 50 mT using a permanent magnet Halbach array. *Magn Reson Med*. 2021;85(1):495-505.

16) Sarracanie M, LaPierre CD, Salameh N, Waddington DEJ, Witzel T, Rosen MS. Low-Cost High-Performance MRI. *Sci Rep*. 2015;5:15177.

17) Hamilton-Basich M. Hyperfine Receives FDA Clearance for Portable MRI Technology. *AXIS Imaging News; Overland Park*. Published online August 16, 2020. https://search.proquest.com/openview/5c609d9987037cd3e2d4e866bfbc9ad0/1?pq-origsite=gscholar&cbl=2037571.

18) Panther A, Thevathasen G, Connell IRO, et al. A dedicated head-only MRI scanner for point-of-care imaging. In: *ISMRM 27th Annual Meeting & Exhibition*. ; 2019. https://www.synaptivemedical.com/wp-content/uploads/2020/04/a-dedicated-head-only-mri-scanner-for-point-of-care-imaging.pdf

19) Chiragzada S, Hellman E, Michael D, Narayanan R, Nacev A, Kumar D. Initial phantom studies for an office-based low-field MR system for prostate biopsy. *Int J Comput Assist Radiol Surg*. 2021;16(5):741-748.

20) Ghazinoor S, Crues JV 3rd, Crowley C. Low-field musculoskeletal MRI. *J Magn Reson Imaging*. 2007;25(2):234-244.

21) Klein HM. Low-Field Magnetic Resonance Imaging. *Rofo*. 2020;192(6):537-548.

22) Schick F, Pieper CC, Kupczyk P, et al. 1.5 vs 3 Tesla Magnetic Resonance Imaging: A Review of Favorite Clinical Applications for Both Field Strengths-Part 1. *Invest Radiol*. 2021;56(11):680-691.

23) Hori M, Hagiwara A, Goto M, Wada A, Aoki S. Low-field magnetic resonance imaging: Its history and renaissance. *Invest Radiol*. 2021;56(11):669-679.

24) Heiss R, Nagel AM, Laun FB, Uder M, Bickelhaupt S. Low-Field Magnetic Resonance Imaging: A New Generation of Breakthrough Technology in Clinical Imaging. *Invest Radiol*. 2021;56(11):726-733.

25) Khodarahmi I, Bonham LW, Weiss CR, Fritz J. Needle Heating During Interventional Magnetic Resonance Imaging at 1.5- and 3.0-T Field Strengths. *Invest Radiol*. 2020;55(6):396-404.

26) Runge VM, Heverhagen JT. Advocating the Development of Next-Generation, Advanced-Design Low-Field Magnetic Resonance Systems. *Invest Radiol*. 2020;55(12):747-753.

27) Basar B, Sonmez M, Yildirim DK, et al. Susceptibility artifacts from metallic markers and cardiac catheterization devices on a high-performance 0.55 T MRI system. *Magn Reson Imaging*. 2021;77:14-20.

28) Webb AG. *Magnetic Resonance Technology: Hardware and System Component Design*. Royal Society of Chemistry; 2016.

29) Buckley BW, MacMahon PJ. Radiology and the Climate Crisis: Opportunities and Challenges—Radiology In Training. *Radiology*. 2021;300(3):E339-E341. doi:10.1148/radiol.2021210851

30) Keller PJ, Hunter WW Jr, Schmalbrock P. Multisection fat-water imaging with chemical shift selective presaturation. *Radiology*. 1987;164(2):539-541.

31) Frahm J, Haase A, Hänicke W, Matthaei D, Bomsdorf H, Helzel T. Chemical shift selective MR imaging using a whole-body magnet. *Radiology*. 1985;156(2):441-444. doi:10.1148/radiology.156.2.4011907

32) Campbell-Washburn AE. 2019 American Thoracic Society BEAR Cage Winning Proposal: Lung Imaging Using High-Performance Low-Field Magnetic Resonance Imaging. *Am J Respir Crit Care Med*. 2020;201(11):1333-1336.

33) Bhattacharya I, Ramasawmy R, Javed A, et al. Assessment of Lung Structure and Regional Function Using 0.55 T MRI in Patients With Lymphangioleiomyomatosis. *Invest Radiol*. 2022;57(3):178-186.

34) Bhattacharya I, Ramasawmy R, Javed A, et al. Oxygen-enhanced functional lung imaging using a contemporary 0.55 T MRI system. *NMR in Biomedicine*. 2021;34(8). doi:10.1002/nbm.4562

35) Javed A, Ramasawmy R, O'Brien K, et al. Self-gated 3D stack-of-spirals UTE pulmonary imaging at 0.55T. *Magn Reson Med*. 2022;87(4):1784-1798.

36) Campbell-Washburn AE, Suffredini AF, Chen MY. High-Performance 0.55-T Lung MRI in Patient with COVID-19 Infection. *Radiology*. 2021;299(2):E246-E247. doi:10.1148/radiol.2021204155

37) Heiss R, Grodzki DM, Horger W, Uder M, Nagel AM, Bickelhaupt S. High-performance low field MRI enables visualization of persistent pulmonary damage after COVID-19. *Magn Reson Imaging*. 2021;76:49-51.

38) Campbell-Washburn AE, Malayeri AA. T2-weighted lung imaging using a 0.55-T MRI system. *Radiology*. Published online 2021. https://pubs.rsna.org/doi/abs/10.1148/ryct.2021200611

39) Bandettini WP, Shanbhag SM, Mancini C, et al. Evaluation of myocardial infarction by cardiovascular magnetic resonance at 0.55-T compared to 1.5-T. *JACC Cardiovasc Imaging*. 2021;14(9):1866-1868.

40) Bandettini WP, Patricia Bandettini W, Shanbhag SM, et al. A comparison of cine CMR imaging at 0.55 T and 1.5 T. *Journal of Cardiovascular Magnetic Resonance*. 2020;22(1). doi:10.1186/s12968-020-00618-y

41) Amin EK, Campbell-Washburn A, Ratnayaka K. MRI-Guided Cardiac Catheterization in Congenital Heart Disease: How to Get Started. *Curr Cardiol Rep*. Published online February 2, 2022. doi:10.1007/s11886-022-01659-8

42) Tavernier T, Cotten A. High- Versus Low-Field MR Imaging. *Radiologic Clinics of North America*. 2005;43(4):673-681. doi:10.1016/j.rcl.2005.02.001

43) Riel KA, Reinisch M, Kersting-Sommerhoff B, Hof N, Merl T. 0.2-Tesla magnetic resonance imaging of internal lesions of the knee joint: a prospective arthroscopically controlled clinical study. *Knee Surgery, Sports Traumatology, Arthroscopy*. 1999;7(1):37-41. doi:10.1007/s001670050118

44) Van Speybroeck CDE, O'Reilly T, Teeuwisse W, Arnold PM, Webb AG. Characterization of displacement forces and image artifacts in the presence of passive medical implants in low-field (<100 mT) permanent magnet-based MRI systems, and comparisons with clinical MRI systems. *Physica Medica*. 2021;84:116-124. doi:10.1016/j.ejmp.2021.04.003

45) Chandarana H, Bagga B, Huang C, et al. Diagnostic abdominal MR imaging on a prototype low-field 0.55 T scanner operating at two different gradient strengths. *Abdom Radiol (NY)*. 2021;46(12):5772-5780.

46) Campbell-Washburn AE, Mancini C, Conrey A, et al. Evaluation of hepatic iron overload using a contemporary 0.55 T MRI system. *J Magn Reson Imaging*. 2022;55(6):1855-1863.

47) Deoni SCL, Medeiros P, Deoni AT, et al. Development of a mobile low-field MRI scanner. *Sci Rep*. 2022;12(1):5690.

48) Sheth KN, Mazurek MH, Yuen MM, et al. Assessment of Brain Injury Using Portable, Low-Field Magnetic Resonance Imaging at the Bedside of Critically Ill Patients. *JAMA Neurol*. Published online September 8, 2020. doi:10.1001/jamaneurol.2020.3263

49) Shah J, Cahn B, By S, et al. Portable, Bedside, Low-field Magnetic Resonance Imaging in an Intensive Care Setting for Intracranial Hemorrhage (270). *Neurology*. 2020;94(15 Supplement). Accessed March 5, 2022. https://n.neurology.org/content/94/15_Supplement/270.abstract

50) Moser E, Laistler E, Schmitt F, Kontaxis G. Ultra-High Field NMR and MRI—The Role of Magnet Technology to Increase Sensitivity and Specificity. *Frontiers in Physics*. 2017;5. doi:10.3389/fphy.2017.00033

51) Robitaille PML, Abduljalil AM, Kangarlu A. Ultra high resolution imaging of the human head at 8 tesla: 2K× 2K for Y2K. *J Comput Assist Tomogr*. 2000;24(1):2-8.

52) Yacoub E, Shmuel A, Pfeuffer J, et al. Imaging brain function in humans at 7 Tesla. *Magn Reson Med*. 2001;45(4):588-594.

53) Robitaille PM, Abduljalil AM, Kangarlu A, et al. Human magnetic resonance imaging at 8 T. *NMR Biomed*. 1998;11(6):263-265.

54) Fda U. Criteria for Significant Risk Investigations of Magnetic Resonance Diagnostic Devices—Guidance for Industry and Food and Drug Administration Staff. Published online 2014.

55) Office of the Commissioner. FDA clears first 7T magnetic resonance imaging device. U.S. Food and Drug Administration. Published October 12, 2017. Accessed February 19, 2022. https://www.fda.gov/news-events/press-announcements/fda-clears-first-7t-magnetic-resonance-imaging-device

56) Ertürk MA, Wu X, Eryaman Y, et al. Toward imaging the body at 10.5 tesla. *Magn Reson Med*. 2017;77(1):434-443.

57) Le Bihan D, Schild T. Human brain MRI at 500 MHz, scientific perspectives and technological challenges. *Supercond Sci Technol*. 2017;30(3):033003.

58) Polimeni JR, Uludağ K. Neuroimaging with ultra-high field MRI: Present and future. *Neuroimage*. 2018;168:1-6.

59) Wu W, Miller KL. Image formation in diffusion MRI: A review of recent technical developments. *J Magn Reson Imaging*. 2017;46(3):646-662.

60) Abduljalil AM, Schmalbrock P, Novak V, Chakeres DW. Enhanced gray and white matter contrast of phase susceptibility-weighted images in ultra-high-field magnetic resonance imaging. *J Magn Reson Imaging*. 2003;18(3):284-290.

61) Polonara G, Scarabino T, Salvolini U. Basics and New Frontiers of MR Spectroscopy with High Tesla. *Rivista di Neuroradiologia*. 2003;16(2_suppl_part2):144-148.

62) de Bazelaire C, Rofsky NM, Duhamel G, et al. Combined T2* and T1 measurements for improved perfusion and permeability studies in high field using dynamic contrast enhancement. *Eur Radiol*. 2006;16(9):2083-2091.

63) Dula AN, Smith SA, Gore JC. Application of Chemical Exchange Saturation Transfer (CEST) MRI for Endogenous Contrast at 7 Tesla. *Journal of Neuroimaging*. 2013;23(4):526-532. doi:10.1111/j.1552-6569.2012.00751.x

64) Öz G, Deelchand DK, Wijnen JP, et al. Advanced single voxel 1 H magnetic resonance spectroscopy techniques in humans: Experts' consensus recommendations. *NMR Biomed*. 2020;34(5):e4236.

65) Niesporek SC, Nagel AM, Platt T. Multinuclear MRI at Ultrahigh Fields. *Top Magn Reson Imaging*. 2019;28(3):173-188.

66) Platt T, Ladd ME, Paech D. 7 Tesla and Beyond: Advanced Methods and Clinical Applications in Magnetic Resonance Imaging. *Invest Radiol*. 2021;56(11):705-725.

67) Andre JB, Bresnahan BW, Mossa-Basha M, et al. Toward Quantifying the Prevalence, Severity, and Cost Associated With Patient Motion During Clinical MR Examinations. *J Am Coll Radiol*. 2015;12(7):689-695.

68) Federau C, Gallichan D. Motion-Correction Enabled Ultra-High Resolution In-Vivo 7T-MRI of the Brain. *PLoS One*. 2016;11(5):e0154974.

69) Mattern H, Sciarra A, Lüsebrink F, Acosta-Cabronero J, Speck O. Prospective motion correction improves high-resolution quantitative susceptibility mapping at 7T. *Magn Reson Med*. 2019;81(3):1605-1619.

70) Schallmo MP, Weldon KB, Burton PC, Sponheim SR, Olman CA. Assessing methods for geometric distortion compensation in 7T gradient echo fMRI data. *bioRxiv*. Published online March 10, 2021:2020.07.02.184515. doi:10.1101/2020.07.02.184515

71) Yamamoto T, Fukunaga M, Sugawara SK, Hamano YH, Sadato N. Quantitative evaluations of geometrical distortion corrections in cortical surface-based analysis of high-resolution functional MRI data at 7T. *J Magn Reson Imaging*. 2021;53(4):1220-1234.

72) Heilmaier C, Theysohn JM, Maderwald S, Kraff O, Ladd ME, Ladd SC. A large-scale study on subjective perception of discomfort during 7 and 1.5 T MRI examinations. *Bioelectromagnetics*. 2011;32(8):610-619. doi:10.1002/bem.20680

73) Rauschenberg J, Nagel AM, Ladd SC, et al. Multicenter Study of Subjective Acceptance During Magnetic Resonance Imaging at 7 and 9.4 T. *Invest Radiol*. 2014;49(5):249.

74) Krug JW, Rose G, Clifford GD, Oster J. ECG-based gating in ultra high field cardiovascular magnetic resonance using an independent component analysis approach. *J Cardiovasc Magn Reson*. 2013;15:104.

75) Chen I, Saha S. Analysis of an Intensive Magnetic Field on Blood Flow. *Electromagnetic Biology and Medicine*. 1984;3(1):293-298. doi:10.3109/15368378409035972

76) Atkinson IC, Renteria L, Burd H, Pliskin NH, Thulborn KR. Safety of human MRI at static fields above the FDA 8 T guideline: sodium imaging at 9.4 T does not affect vital signs or cognitive ability. *J Magn Reson Imaging*. 2007;26(5):1222-1227.

77) Eryaman Y, Zhang P, Utecht L, et al. Investigating the physiological effects of 10.5 Tesla static field exposure on anesthetized swine. *Magn Reson Med*. 2018;79(1):511-514.

78) Heinrich A, Szostek A, Meyer P, et al. Cognition and sensation in very high static magnetic fields: a randomized case-crossover study with different field strengths. *Radiology*. 2013;266(1):236-245.

79) Lepsien J, Müller K, von Cramon DY, Möller HE. Investigation of higher-order cognitive functions during exposure to a high static magnetic field. *J Magn Reson Imaging*. 2012;36(4):835-840.

80) Vocht F de, de Vocht F, Stevens T, et al. Cognitive effects of head-movements in stray fields generated by a 7 Tesla whole-body MRI magnet. *Bioelectromagnetics*. 2007;28(4):247-255. doi:10.1002/bem.20311

81) van Nierop LE, Slottje P, van Zandvoort MJE, de Vocht F, Kromhout H. Effects of magnetic stray fields from a 7 Tesla MRI scanner on neurocognition: a double-blind randomised crossover study. *Occupational and Environmental Medicine*. 2012;69(10):759-766. doi:10.1136/oemed-2011-100468

82) International Commission on Non-Ionizing Radiation Protection (ICNIRP). ICNIRP Statement on Diagnostic Devices Using Non-ionizing Radiation: Existing Regulations and Potential Health Risks. *Health Phys*. 2017;112(3):305.

83) Fatahi M, Reddig A, Friebe B, Reinhold D, Speck O. MRI and Genetic Damage: An Update. *Current Radiology Reports*. 2017;5(6):20.

84) Lancellotti P, Nchimi A, Delierneux C, et al. Biological Effects of Cardiac Magnetic Resonance on Human Blood Cells. *Circ Cardiovasc Imaging*. 2015;8(9):e003697.

85) Reddig A, Fatahi M, Roggenbuck D, et al. Impact of in Vivo High-Field-Strength and Ultra-High-Field-Strength MR Imaging on DNA Double-Strand-Break Formation in Human Lymphocytes. *Radiology*. 2017;282(3):782-789.

86) Reddig A, Fatahi M, Friebe B, et al. Analysis of DNA Double-Strand Breaks and Cytotoxicity after 7 Tesla Magnetic Resonance Imaging of Isolated Human Lymphocytes. *PLoS One*. 2015;10(7):e0132702.

87) Foster KR, Moulder JE, Budinger TF. Will an MRI Examination Damage Your Genes? *Radiat Res*. 2017;187(1):1-6.

88) Warner R. Ultra-high field magnets for whole-body MRI. *Supercond Sci Technol*. 2016;29(9):094006.

89) Moser E. Ultra-high-field magnetic resonance: Why and when? *World J Radiol*. 2010;2(1):37-40.

90) Springer E, Dymerska B, Cardoso PL, et al. Comparison of Routine Brain Imaging at 3 T and 7 T. *Invest Radiol*. 2016;51(8):469-482.

91) Straub S, Knowles BR, Flassbeck S, Steiger R, Ladd ME, Gizewski ER. Mapping the human brainstem: Brain nuclei and fiber tracts at 3 T and 7 T. *NMR Biomed*. 2019;32(9):e4118.

92) Wrede KH, Dammann P, Johst S, et al. Non-Enhanced MR Imaging of Cerebral Arteriovenous Malformations at 7 Tesla. *Eur Radiol*. 2016;26(3):829-839.

93) Wrede KH, Matsushige T, Goericke SL, et al. Non-enhanced magnetic resonance imaging of unruptured intracranial aneurysms at 7 Tesla: Comparison with digital subtraction angiography. *Eur Radiol*. 2017;27(1):354-364.

94) Novak V, Abduljalil AM, Novak P, Robitaille PM. High-resolution ultrahigh-field MRI of stroke. *Magn Reson Imaging*. 2005;23(4):539-548.

95) Bruschi N, Boffa G, Inglese M. Ultra-high-field 7-T MRI in multiple sclerosis and other demyelinating diseases: from pathology to clinical practice. *Eur Radiol Exp*. 2020;4(1):59.

96) Wisse LEM, Biessels GJ, Heringa SM, et al. Hippocampal subfield volumes at 7T in early Alzheimer's disease and normal aging. *Neurobiol Aging*. 2014;35(9):2039-2045.

97) Lehéricy S, Bardinet E, Poupon C, Vidailhet M, François C. 7 Tesla magnetic resonance imaging: a closer look at substantia nigra anatomy in Parkinson's disease. *Mov Disord*. 2014;29(13):1574-1581.

98) Wang I, Oh S, Blümcke I, et al. Value of 7T MRI and post-processing in patients with nonlesional 3T MRI undergoing epilepsy presurgical evaluation. *Epilepsia*. 2020;61(11):2509-2520.

99) Opheim G, van der Kolk A, Markenroth Bloch K, et al. 7T Epilepsy Task Force Consensus Recommendations on the Use of 7T MRI in Clinical Practice. *Neurology*. 2021;96(7):327-341.

100) Regnery S, Knowles BR, Paech D, et al. High-resolution FLAIR MRI at 7 Tesla for treatment planning in glioblastoma patients. *Radiother Oncol*. 2019;130:180-184.

101) 1Chang G, Pakin SK, Schweitzer ME, Saha PK, Regatte RR. Adaptations in trabecular bone microarchitecture in Olympic athletes determined by 7T MRI. *J Magn Reson Imaging*. 2008;27(5):1089-1095.

102) Springer E, Bohndorf K, Juras V, et al. Comparison of routine knee magnetic resonance imaging at 3 T and 7 T. *Invest Radiol*. 2017;52(1):42-54.

103) Lazik A, Theysohn JM, Geis C, et al. 7 Tesla quantitative hip MRI: T1, T2 and T2* mapping of hip cartilage in healthy volunteers. *Eur Radiol*. 2016;26(5):1245-1253.

104) Wyatt C, Guha A, Venkatachari A, et al. Improved differentiation between knees with cartilage lesions and controls using 7T relaxation time mapping. *J Orthop Translat*. 2015;3(4):197-204.

105) Wu B, Wang C, Krug R, et al. 7T human spine imaging arrays with adjustable inductive decoupling. *IEEE Trans Biomed Eng*. 2010;57(2):397-403.

106) Rietsch SHG, Brunheim S, Orzada S, et al. Development and evaluation of a 16-channel receive-only RF coil to improve 7T ultra-high field body MRI with focus on the spine. *Magn Reson Med*. 2019;82(2):796-810.

107) Laader A, Beiderwellen K, Kraff O, et al. 1.5 versus 3 versus 7 Tesla in abdominal MRI: A comparative study. *PLoS One*. 2017;12(11):e0187528.

108) Umutlu L, Orzada S, Kinner S, et al. Renal imaging at 7 Tesla: preliminary results. *Eur Radiol*. 2011;21(4):841-849.

109) Fischer A, Kraff O, Orzada S, et al. Ultra-high-Field Imaging of the Biliary Tract at 7 T: Initial Results of Gadoxetic Acid–Enhanced Magnetic Resonance Cholangiography. *Invest Radiol*. 2014;49(5):346.

110) Vos EK, Lagemaat MW, Barentsz JO, et al. Image quality and cancer visibility of T2-weighted magnetic resonance imaging of the prostate at 7 Tesla. *Eur Radiol*. 2014;24(8):1950-1958.

111) Kraff O, Quick HH. 7T: Physics, safety, and potential clinical applications. *J Magn Reson Imaging*. 2017;46(6):1573-1589.

112) Stehouwer BL, Klomp DWJ, van den Bosch MAAJ, et al. Dynamic contrast-enhanced and ultra-high-resolution breast MRI at 7.0 Tesla. *Eur Radiol*. 2013;23(11):2961-2968.

113) von Knobelsdorff-Brenkenhoff F, Tkachenko V, Winter L, et al. Assessment of the right ventricle with cardiovascular magnetic resonance at 7 Tesla. *J Cardiovasc Magn Reson*. 2013;15:23.

Improving Radiology Resident Proficiency in MRI Safety

Akarshan Monga, DO[1]; Shima Aran, MD[2]

Abstract

Background: Radiology residents are often tasked with deciding whether a patient can safely undergo a magnetic resonance (MRI) imaging scan. To correctly make these decisions the residents need to have strong knowledge about MRI safety issues. There are gaps in radiology resident knowledge about MRI safety that might be addressed with a variety of educational interventions.

Objective and hypothesis*:* The primary objective of this project is to increase mean radiology resident knowledge about MRI safety by a statistically significant amount. The null hypothesis is that mean pre- and post-intervention knowledge scores will be the same, and the alternative hypothesis is that mean post-intervention score will be greater.

Methods: We assessed baseline MRI safety knowledge of Detroit Medical Center radiology residents (number=35) with a 10 question quiz. The radiology residents were then provided a PowerPoint presentation that summarizes recent review articles about MRI safety. Next, the residents took the same quiz again. We compared the pre- and post-intervention quiz scores.

Results*:* 10 radiology residents (28.6%) completed the pre-quiz and 9 radiology residents (25.7%) completed the post-quiz. When comparing the pre- and post-intervention quiz scores, the t stat = -2.020 and p one-tail= 0.03. As $p < 0.05$, the null hypothesis is rejected, and we can conclude that mean post-quiz score > pre-quiz score with statistical significance.

Conclusion*:* There was a statistically significant increase in mean quiz score after residents reviewed a PowerPoint on MRI safety. Therefore, we achieved the primary objective by increasing resident knowledge about MRI safety. The participating residents can now make decisions about MRI safety with more accuracy and confidence. The primary limitation of this study was that fewer than 30% of the radiology residents participated and the respondents were skewed towards the early training years.

Affiliations: [1]Department of Radiology, Detroit Medical Center, Detroit, Michigan. [2]Department of Radiology, Detroit Medical Center, Detroit, Michigan and the Department of Radiology, McGovern Medical School, The University of Texas Health Science Center, Houston, Texas.
Conflict of interest and support statement: The authors declare no conflicts of interest and no sources of support.
Data availability statement: All data relevant to the study are provided in the article or supplement.
Prior presentation: Monga A, Aran S. Improving Radiology Resident Proficiency in MR Safety. Poster presented at: 2021 DMC GME QuESST Resident Research Day Poster Competition; April 21-26, 2021; Detroit, MI.

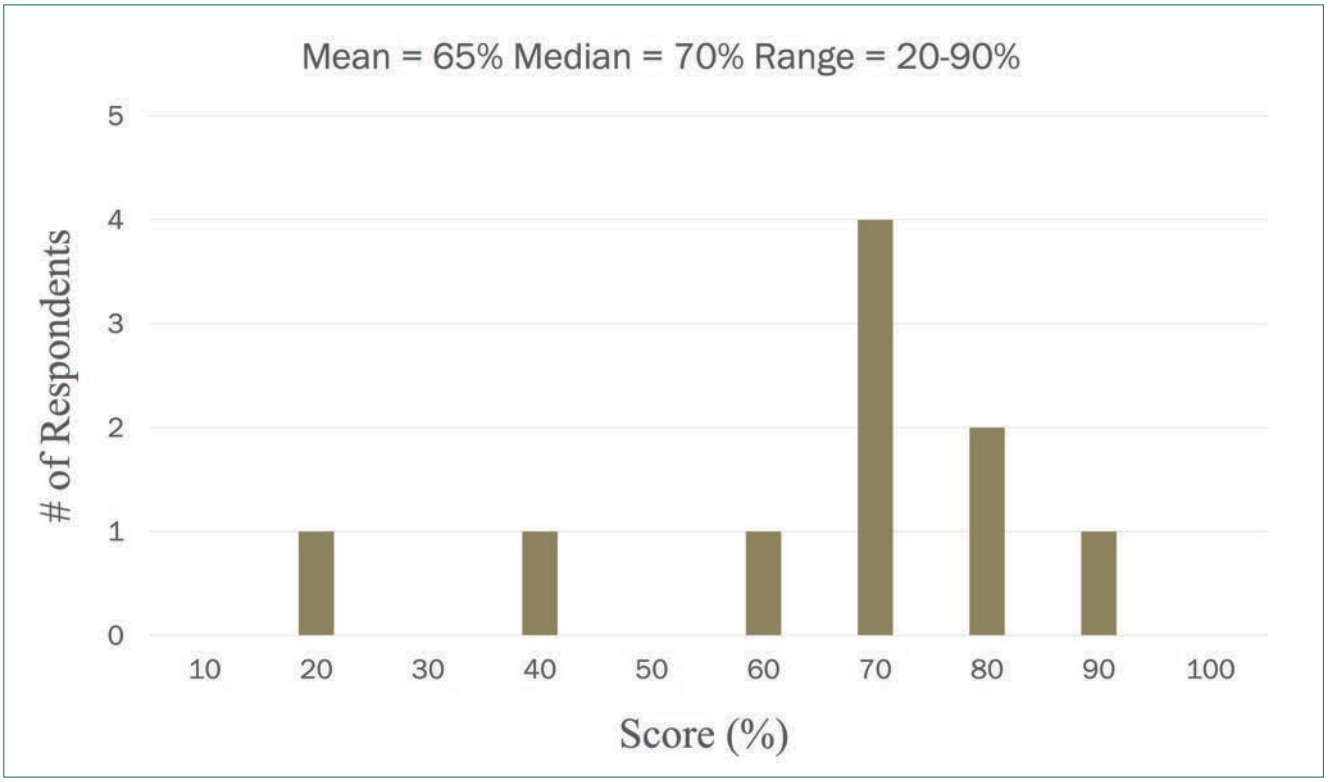

Figure 1. Pre-intervention quiz results.

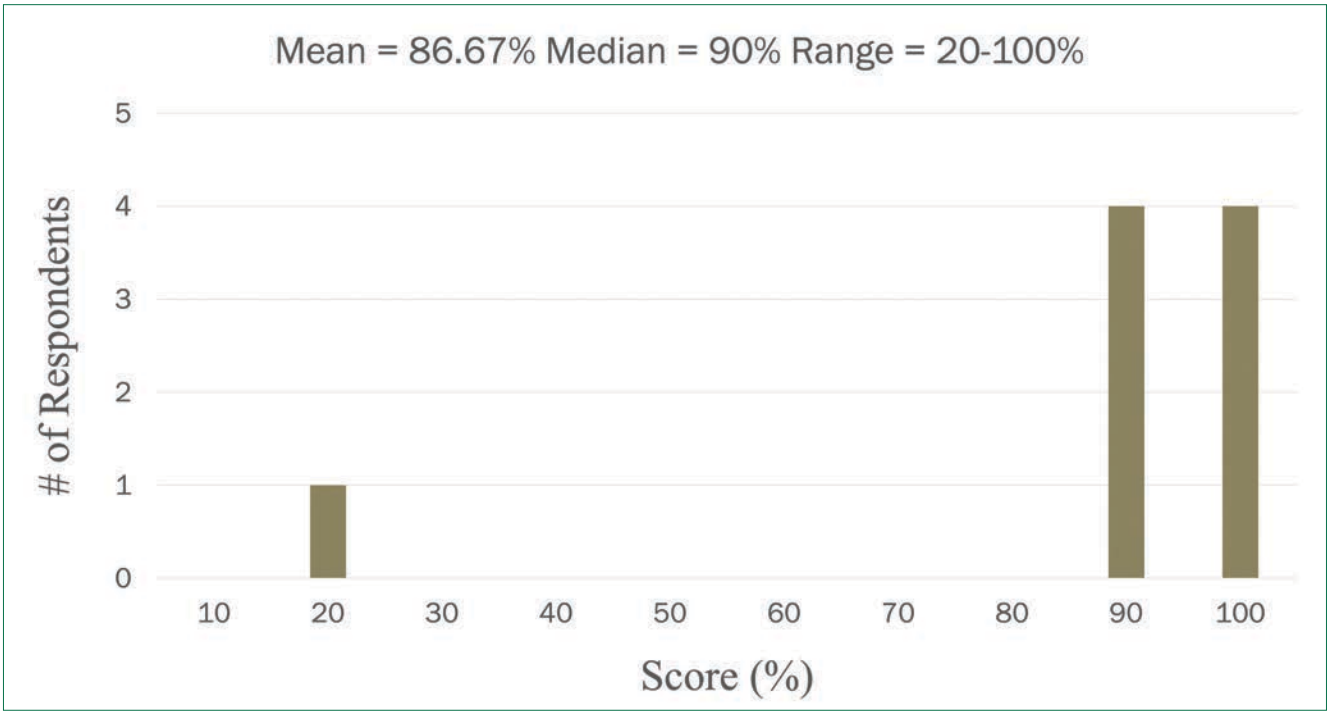

Figure 2. Post-intervention quiz results.

Introduction

There are multiple patient safety issues associated with MRI imaging due to the strong magnetic field and rapidly changing gradients, as well as concerns about administration of gadolinium-based contrast agents. The MRI technologist or radiology nursing staff frequently contact on-call radiology residents to resolve their concerns and specifically to ask whether a patient can be safely scanned or can safely receive contrast. Hollingsworth, et al,[1] found gaps in radiology resident knowledge about these issues. Swenson, et al,[2] assessed whether online modules or live lectures would improve resident knowledge about MRI safety and found statistically significant improvement in resident knowledge after intervention with both online modules and live lectures.

The primary objective of this project is to increase mean radiology resident knowledge about MRI safety by a statistically significant amount. The null hypothesis is that mean pre- and post-intervention scores will be the same, and the alternative hypothesis is that mean post-intervention score will be greater.

The secondary objective of this project is to decrease radiology resident decision making time about MRI safety issues by a statistically significant amount. The null hypothesis is that mean pre- and post-intervention time to complete the quiz will be the same, and the alternative hypothesis is that mean post-intervention time will be less.

Many benefits will result from the achievement of these objectives. Patients will benefit from more accurate MRI safety decisions. MRI safety decisions will be made more accurately and faster, helping patient management decisions by ordering physicians. Radiology residents will gain accuracy, speed, and confidence when making decisions.

Methods and Materials

We assessed baseline knowledge of Detroit Medical Center radiology residents (number=35) with a quiz of 10 multiple choice questions about the topics of MRI magnet and contrast safety. The quiz included an additional question asking how long it took the respondent to complete the quiz. We also asked the residents their current training year. Residents were not asked to identify themselves and the scores were anonymous. The radiology residents were then provided a 17-slide PowerPoint presentation file that summarizes recent review articles [3,4] about MRI safety. Residents had the opportunity to download and self-review the PowerPoint file. The topics covered in the PowerPoint presentation included: basic MRI physics, medical device and implant MRI compatibility, regulations regarding maximum specific absorption rate and acoustic levels, assessment of risk of nephrogenic systemic fibrosis and other issues related to the use of IV gadolinium, MRI safety zones, and management of emergencies near the scanner. Next, the residents retook the same quiz. Time delays between the preintervention quiz, reviewing the PowerPoint and then retesting were not specified and the residents self-selected when they retook the post-intervention quiz. We compared the mean of the pre- and post-intervention quiz scores and time to complete using t-tests.

Results

10 radiology residents (28.6%) completed the pre-quiz, which included 4 first-year, 3 second-year, 2 third-year, and 1 fourth-year residents. 9 radiology residents (25.7%) completed the post-quiz, which included 4 first-year, 2 second-year, 2 third-year, and 1 fourth-year residents. See Figures 1 and 2 for quiz scores. Regarding the quiz scores, the t stat = -2.020 and p one-tail= 0.03. As $p < 0.05$, the null hypothesis is rejected, and we can conclude that mean post-quiz score > pre-quiz score with statistical significance.

As for the time to complete the quiz, for the pre-quiz, mean = 5.2 minutes, median = 5 minutes, and the range = 2-10 minutes. For the post-quiz, the mean = 2.44 minutes, median = 2 minutes, and range = 1-5 minutes. The t stat = 3.41 and p one-tail= 0.002. As $p < 0.05$, the null hypothesis is rejected, and we can conclude that mean post-quiz time to complete < mean pre-quiz time to complete with statistical significance.

Discussion

There was a statistically significant increase in mean quiz score after residents reviewed a PowerPoint on MRI safety. Therefore, we achieved the primary objective by increasing resident knowledge about MRI safety. Additionally, we found a statistically significant decrease in time to complete the quiz after the intervention. As such, the secondary objective to improve resident speed in answering questions about MRI safety issues was also achieved, suggesting that they now knew the correct answer. The participating residents will likely be able to make decisions about MRI safety with more accuracy and with improved speed and confidence.

One limitation of this study is that fewer than 30% of the radiology residents participated and the respondents were skewed towards

the early training years. This may have impacted the results as intervention would be expected to result in greater increase in knowledge for less experienced residents. Additionally, there was no specific time delay between reviewing the PowerPoint, and the post-quiz, so that long term and intermediate term retention were not assessed. As the scores were anonymous, individual improvement could not be assessed and only mean changes were assessed.

As a next step we can further improve resident knowledge on this topic through different education tools such as modules, lectures, and training/simulations.

References

1) Hollingsworth TD, Duszak R Jr, Vijayasarathi A, Gelbard RB, Mullins ME. Trainee knowledge of imaging appropriateness and safety: results of a series of surveys from a large academic medical center. *Curr Probl Diagn Radiol.* 2019;48(1):17-21. doi:10.1067/j.cpradiol.2017.10.007

2) Swensson J, McMahan L, Rase B, Tahir B. Curricula for teaching MRI Safety, and MRI and CT contrast safety to residents: how effective are live lectures and online modules?. *J Am Coll Radiol.* 2015;12(10):1093-1096. doi:10.1016/j.jacr.2015.04.012

3) Tsai LL, Grant AK, Mortele KJ, Kung JW, Smith MP. A practical guide to MR imaging safety: what radiologists need to know. *Radiographics.* 2015;35(6):1722-1737. doi:10.1148/rg.2015150108

4) Kim SJ, Kim KA. Safety issues and updates under MR environments. *Eur J Radiol.* 2017;89:7-13. doi:10.1016/j.ejrad.2017.01.010


Applied
Radiology

The 2023 Leaders on the Horizon Residents' Program

This exclusive program is designed to identify, cultivate, and highlight the future stars in medical imaging.

All radiology residents are invited to submit a clinical research article and/or a clinical review paper, which will be considered for publication in a special supplement to *Applied Radiology.*

Topics should be focused on imaging modalities and/or areas related to medical imaging.

Residents authoring the top three (3) clinical research papers and the top three (3) clinical review articles will:

- Win a trip to RSNA 2023
- Get published in a special supplement to *Applied Radiology*
- Receive a scholarship award to support their educational endeavors

Scholarship Awards

Clinical Research Papers		**Clinical Review Papers**	
1st place	$7500	1st place	$3000
2nd place	$5000	2nd place	$2000
3rd place	$3000	3rd place	$1000

Submission Deadline: October 1, 2023

To register visit appliedradiology.com/leaders

This educational opportunity is supported by Bracco Diagnostics, Inc.

BRACCO

LIFE FROM INSIDE

LIFE FROM INSIDE